N91-14477

ABSTRACT

The diffraction by a material discontinuity in a thick dielectric/ferrite layer is considered by modelling the layer as a distributed current sheet obeying generalized sheet transition conditions (GSTCs). The sheet currents are then formulated and solved via the standard dual integral equation approach. This yields the diffracted field in terms of unknown constants which underscore the non-uniqueness of the GSTC current sheet representation. The constants are dependent on the geometry and properties of the discontinuity and are determined by enforcing field continuity across the material junction. This requires the field internal to the slab which are determined from the external ones via analytic continuity. Results are given which validate the solution and demonstrate the importance of the constants.

OBJECTIVE

This task involves the use of higher order boundary conditions to generate new solutions in diffraction theory. In particular, diffraction coefficients will be developed for dielectric/magnetic layers and metal-dielectric junctions which are often encountered on airborne vehicles as terminations of coatings and conformal antennas. Solutions for both polarizations will be developed for fairly thick junctions and versatile computer codes will be written and tested. Creeping wave diffraction coefficients will be also developed for multilayered coated cylinders.

PROGRESS

1 Introduction

In scattering, layered materials are often modeled by equivalent sheets satisfying simple boundary/transition conditions. In particular, impenetrable layers are typically replaced by opaque sheets satisfying standard impedance boundary conditions (SIBCs) [1], whereas penetrable layers are

represented by transparent sheets obeying resistive or conductive type transition conditions (STCs) [2]. These simple boundary/transition conditions relate the normal fields to their first normal derivatives through proportionality factors, "impedances" in the SIBC case and "resistivities/conductivities" in the STC case. With this modeling scheme, a discontinuity in layered material is represented by an equivalent sheet discontinuity, whose scattering may be treated via function theoretic techniques such as the Wiener-Hopf method. As is well known, however, these equivalent sheet representations are valid only for very thin or lossy layers and alternative simulations are therefore required to model discontinuities in low loss layers and/or layers of appreciable thickness.

One such approach is to employ generalized impedance boundary conditions (GIBCs) [3] [4] or generalized sheet transition conditions (GSTCs) [5] [6] in place of the usual SIBCs and STCs. The GIBCs and GSTCs are respective generalizations of SIBCs and STCs and permit a more accurate representation of the fields at the surface of the coating or layer. Unlike the SIBCs or STCs, GIBCs and GSTCs include second and possibly higher order derivatives of the field components on the equivalent sheet which are responsible for the higher accuracy of the conditions. The highest derivative kept in the condition defines their order and generally the accuracy of the conditions is analogous to the order. As can be expected, thicker and multilayer coatings require higher order conditions for an accurate simulation and to date a plethora of GIBCs and GSTCs have been derived to model a variety of material coatings and layers [6] [7] [8] [9] [10].

GIBC/GSTC sheets are well suited for characterizing the diffraction by discontinuities in thick coatings or layers. In particular, they can be employed in conjunction with the Wiener-Hopf method or dual integral equation approach without much deviation from the procedure used in connection with the SIBC or STC conditions. However, the resulting solutions obtained in this manner are inherently non-unique [11] [12]. This non-uniqueness cannot be removed with the usual application of the edge condition or the enforcement of reciprocity, which has been used in the past to generate a more physically appealing, if not a unique, solution.

Uniqueness is an obvious requirement of the physical problem and unless resolved it would seriously undermine the usefulness of the conditions. In the case at hand, the non-uniqueness is manifested in the form of unknown

solution constants [12] and this simply points to the fact that additional conditions are required for their specification.

In this paper we demonstrate that the GIBC/GSTC sheet characterization can yield a complete solution when supplemented with certain conditions at the sheet discontinuity which do not require apriori knowledge of the edge fields. As a vehicle in presenting this solution procedure we employ the dual integral equation method to consider the plane wave diffraction by a discontinuous distributed sheet (see Figure 1(b)). This very general model is capable of representing material half-planes, material junctions, and material discontinuities on grounded structures, such as those shown in Figure 2. In addition, a distributed sheet model typically renders the same degree of accuracy as the usual infinitely-thin sheet, but with a lower order condition. It is, therefore, of much practical interest.

In the first part of the paper, the GSTC representation of the distributed sheet discontinuity is used to develop dual integral equations in terms of the unknown spectral functions proportional to the sheet currents. These equations are then solved in the standard manner to yield expressions for the spectral functions in terms of unknown constants, and examples are presented where a proper choice for the constants demonstrates that they recover known solutions. This demonstrates the validity of the presented solution, but in general, the determination of the constants requires the enforcement of additional constraints demanding field continuity across the junction. The development of these conditions and their use in solving for the constants is also presented.

2 Dual Integral Equation Formulation

Consider a distributed sheet of thickness τ illuminated by the plane wave

$$F_{inc} = e^{jk(x\cos\phi_o + y\sin\phi_o)} = \begin{cases} E_{z,inc}, & E_z \text{ polarization}, \\ Z_o H_{z,inc}, & H_z \text{ polarization}, \end{cases} \tag{1}$$

as shown in Figure 1(a). The excitation (1) induces reflected and transmitted fields which are explicitly given by the properties of the distributed sheet. If this sheet models a symmetric slab, then an appropriate GSTC

representation is formally given by [10]

$$\mathcal{U}_{11}^1\left(-\frac{\partial x^2}{k^2}\right)\left\{F^+ - F^-\right\} + \frac{j}{k}\mathcal{U}_{12}^1\left(-\frac{\partial x^2}{k^2}\right)\left\{\partial y\left[F^+ + F^-\right]\right\} = 0,$$

$$-\infty < x < \infty$$

$$\mathcal{U}_{21}^1\left(-\frac{\partial x^2}{k^2}\right)\left\{F^+ + F^-\right\} + \frac{j}{k}\mathcal{U}_{22}^1\left(-\frac{\partial x^2}{k^2}\right)\left\{\partial y\left[F^+ - F^-\right]\right\} = 0,$$

$$-\infty < x < \infty. \qquad (2)$$

in which F is the total field, $F^{\pm} = F(x, y = \pm\tau/2)$, $\partial x F^{\pm} = \frac{\partial}{\partial x}F(x, y = \pm\tau/2)$, and $\partial y F^{\pm} = \frac{\partial}{\partial y}F(x,y)\,|_{y=\pm\tau/2}$. Also, $\mathcal{U}_{ij}^1\left(-\frac{\partial x^2}{k^2}\right)$ are differential operators which operate on the field quantity in the curly brackets, and are finite polynomials in $-\frac{\partial x^2}{k^2}$ whose coefficients depend on the slab modeled by the distributed sheet. To maintain the generality of the solution, the $\mathcal{U}_{ij}^1$ operators are left in symbolic form and the reader is referred to [10] for their explicit representation in terms of the material constants and thickness of the layers comprising the modeled slab. In general, the order of $\mathcal{U}_{11}^1$ (i.e. the highest derivative present) is usually the same or one more than that of $\mathcal{U}_{12}^1$ and similarly the order of $\mathcal{U}_{21}^1$ is the same or one more than the order of $\mathcal{U}_{22}^1$. Thus, we may define the orders of the GSTCs in (2) to be

$$\begin{aligned} N_1^{odd} &= \text{maximum}\left\{\text{ order of } \mathcal{U}_{11}^1\left(\lambda^2\right), 1 + \text{ order of } \mathcal{U}_{12}^1\left(\lambda^2\right)\right\} \\ N_1^{even} &= \text{maximum}\left\{\text{ order of } \mathcal{U}_{21}^1\left(\lambda^2\right), 1 + \text{ order of } \mathcal{U}_{22}^1\left(\lambda^2\right)\right\} \end{aligned} \qquad (3)$$

The reflected and transmitted fields may now be easily determined by employing (2) to find

$$F_{refl} = R_1 e^{jk(x\cos\phi_o - y\sin\phi_o)} \qquad (4)$$

$$F_{tran} = T_1 e^{jk(x\cos\phi_o + y\sin\phi_o)} \qquad (5)$$

in which R_1 and T_1 are the reflection and transmission coefficients, respectively, and are given as

$$R_1 = \frac{e^{jk\tau\sin\phi_o}}{2}\left[R_1^{even} + R_1^{odd}\right] \qquad (6)$$

$$T_1 = \frac{e^{jk\tau\sin\phi_o}}{2}\left[R_1^{even} - R_1^{odd}\right]. \qquad (7)$$

with

$$R_1^{even} = \frac{\sin\phi_o \mathcal{U}_{22}^1(\cos^2\phi_o) - \mathcal{U}_{21}^1(\cos^2\phi_o)}{\sin\phi_o \mathcal{U}_{22}^1(\cos^2\phi_o) + \mathcal{U}_{21}^1(\cos^2\phi_o)} \tag{8}$$

$$R_1^{odd} = \frac{\sin\phi_o \mathcal{U}_{12}^1(\cos^2\phi_o) - \mathcal{U}_{11}^1(\cos^2\phi_o)}{\sin\phi_o \mathcal{U}_{12}^1(\cos^2\phi_o) + \mathcal{U}_{11}^1(\cos^2\phi_o)}. \tag{9}$$

We remark that in (8) and (9), $\mathcal{U}_{ij}^1(\cos^2\phi_o)$ now represent simple polynomial functions in $\cos^2\phi_o$, since $-\partial x^2/k^2 = \cos^2\phi_o$ in view of the field expressions (4) and (5).

Consider now the case where the right half of the distributed sheet in Figure 1(a) is replaced by another sheet of the same thickness, but of different properties, as illustrated in Figure 1(b). The GSTC representation of this modified sheet is

$$\begin{aligned}
\mathcal{U}_{11}^1\left(-\frac{\partial x^2}{k^2}\right)\left\{F^+ - F^-\right\} + \frac{j}{k}\mathcal{U}_{12}^1\left(-\frac{\partial x^2}{k^2}\right)\left\{\partial y\left[F^+ + F^-\right]\right\} &= 0 \\
\mathcal{U}_{21}^1\left(-\frac{\partial x^2}{k^2}\right)\left\{F^+ + F^-\right\} + \frac{j}{k}\mathcal{U}_{22}^1\left(-\frac{\partial x^2}{k^2}\right)\left\{\partial y\left[F^+ - F^-\right]\right\} &= 0,
\end{aligned} \tag{10}$$

for $-\infty < x < 0$ and

$$\begin{aligned}
\mathcal{U}_{11}^2\left(-\frac{\partial x^2}{k^2}\right)\left\{F^+ - F^-\right\} + \frac{j}{k}\mathcal{U}_{12}^2\left(-\frac{\partial x^2}{k^2}\right)\left\{\partial y\left[F^+ + F^-\right]\right\} &= 0 \\
\mathcal{U}_{21}^2\left(-\frac{\partial x^2}{k^2}\right)\left\{F^+ + F^-\right\} + \frac{j}{k}\mathcal{U}_{22}^2\left(-\frac{\partial x^2}{k^2}\right)\left\{\partial y\left[F^+ - F^-\right]\right\} &= 0,
\end{aligned} \tag{11}$$

for $0 < x < \infty$, where the superscripts 1 and 2 distinguish the left- and right-hand sheets, respectively. Referring to our previous discussion, the orders of the right hand side GSTCs are given as

$$\begin{aligned}
N_2^{odd} &= \max\left\{\text{order of } \mathcal{U}_{11}^2\left(\lambda^2\right) \text{ in } \lambda, 1 + \text{order of } \mathcal{U}_{12}^2\left(\lambda^2\right) \text{ in } \lambda\right\} \\
N_2^{even} &= \max\left\{\text{order of } \mathcal{U}_{21}^2\left(\lambda^2\right) \text{ in } \lambda, 1 + \text{order of } \mathcal{U}_{22}^2\left(\lambda^2\right) \text{ in } \lambda\right\}.
\end{aligned} \tag{12}$$

The modified right hand side sheet induces a scattered field F_s in the presence of the excitation (1), and the total field can be represented as

$$F = \begin{cases} F_{inc} + F_{refl} + F_s & y > \tau/2 \\ F_{tran} + F_s & y < \tau/2 \end{cases} \tag{13}$$

where F_s is the unknown scattered field in the region $|y| > \tau/2$ and can be expressed as [13] [14]

$$\begin{aligned} F^s(x,y) &= \int_C \left[\frac{|y|}{y} P_{odd}(\cos\alpha) + P_{even}(\cos\alpha) \right] \\ &\quad \cdot \; e^{-jk\sin\alpha(|y|-\tau/2)} e^{-jkx\cos\alpha} d\alpha. \end{aligned} \tag{14}$$

where C is a contour in the complex α plane, such that $\lambda = \cos\alpha$ runs from $-\infty$ to ∞ as shown in Figure 3. In this, the spectral functions $P_{odd}(\cos\alpha)$ and $P_{even}(\cos\alpha)$ are directly related to the Fourier transforms of the unknown equivalent currents

$$J_{odd} = F_s^+ - F_s^- \tag{15}$$

$$J_{even} = F_s^+ + F_s^-, \tag{16}$$

via the relations

$$J_{odd}(x) = 2\int_{-\infty}^{\infty} P_{odd}(\lambda)\, e^{-jkx\lambda} \frac{d\lambda}{\sqrt{1-\lambda^2}} \tag{17}$$

$$J_{even}(x) = 2\int_{-\infty}^{\infty} P_{even}(\lambda)\, e^{-jkx\lambda} \frac{d\lambda}{\sqrt{1-\lambda^2}}. \tag{18}$$

Substituting (1), (4), (5), (13) and (14) into the transition conditions (11) and (12), and introducing the transformation $\lambda = \cos\alpha$ (see Figure 3) yields

$$\int_{-\infty}^{\infty} \mathcal{G}_1^{odd}\left(\lambda^2\right) P_{odd}(\lambda)\, e^{-jkx\lambda} \frac{d\lambda}{\sqrt{1-\lambda^2}} = 0 \tag{19}$$

$$\int_{-\infty}^{\infty} \mathcal{G}_1^{even}\left(\lambda^2\right) P_{even}(\lambda)\, e^{-jkx\lambda} \frac{d\lambda}{\sqrt{1-\lambda^2}} = 0, \tag{20}$$

for $x < 0$ and

$$\int_{-\infty}^{\infty} 2\mathcal{G}_2^{odd}\left(\lambda^2\right) P_{odd}\left(\lambda\right) e^{-jkx\lambda} \frac{d\lambda}{\sqrt{1-\lambda^2}}$$

$$= \frac{2\sin\phi_o e^{jkx\lambda_o} e^{jk\tau/2\sin\phi_o} Z_{odd}\left(\lambda_o^2\right)}{\mathcal{G}_1^{odd}\left(\lambda_o^2\right)} \tag{21}$$

$$\int_{-\infty}^{\infty} 2\mathcal{G}_2^{even}\left(\lambda^2\right) P_{even}\left(\lambda\right) e^{-jkx\lambda} \frac{d\lambda}{\sqrt{1-\lambda^2}}$$

$$= \frac{2\sin\phi_o e^{jkx\lambda_o} e^{jk\tau/2\sin\phi_o} Z_{even}\left(\lambda_o^2\right)}{\mathcal{G}_1^{even}\left(\lambda_o^2\right)} \tag{22}$$

for $x > 0$, where $\lambda_o = \cos\phi_o$ and

$$\mathcal{G}_1^{odd}\left(\lambda^2\right) = \mathcal{U}_{11}^1\left(\lambda^2\right) + \sqrt{1-\lambda^2}\mathcal{U}_{12}^1\left(\lambda^2\right) \tag{23}$$

$$\mathcal{G}_1^{even}\left(\lambda^2\right) = \mathcal{U}_{21}^1\left(\lambda^2\right) + \sqrt{1-\lambda^2}\mathcal{U}_{22}^1\left(\lambda^2\right) \tag{24}$$

$$\mathcal{G}_2^{odd}\left(\lambda^2\right) = \mathcal{U}_{11}^2\left(\lambda^2\right) + \sqrt{1-\lambda^2}\mathcal{U}_{12}^2\left(\lambda^2\right) \tag{25}$$

$$\mathcal{G}_2^{even}\left(\lambda^2\right) = \mathcal{U}_{21}^2\left(\lambda^2\right) + \sqrt{1-\lambda^2}\mathcal{U}_{22}^2\left(\lambda^2\right) \tag{26}$$

$$Z_{odd}\left(\lambda_o^2\right) = \left[\mathcal{U}_{11}^1\left(\lambda_o^2\right)\mathcal{U}_{12}^2\left(\lambda_o^2\right) - \mathcal{U}_{12}^1\left(\lambda_o^2\right)\mathcal{U}_{11}^2\left(\lambda_o^2\right)\right] \tag{27}$$

$$Z_{even}\left(\lambda_o^2\right) = \left[\mathcal{U}_{21}^1\left(\lambda_o^2\right)\mathcal{U}_{22}^2\left(\lambda_o^2\right) - \mathcal{U}_{22}^1\left(\lambda_o^2\right)\mathcal{U}_{21}^2\left(\lambda_o^2\right)\right]. \tag{28}$$

Equations (19) with (21) and (20) with (22) form two uncoupled sets of integral equations, sufficient to yield a solution for the unknown spectra $P_{odd}\left(\lambda\right)$ and $P_{even}\left(\lambda\right)$. Clearly, because of the similarity between the two sets of equations, once a solution for $P_{odd}\left(\lambda\right)$ is found, the corresponding one for $P_{even}\left(\lambda\right)$ follows by inspection.

3 Solution of the Diffracted Field

Upon a solution of the dual integral equations (19) and (21) we obtain

$$P_{odd}(\lambda) = \frac{j}{2\pi}\frac{\sin\phi_o\sqrt{1-\lambda^2}}{\lambda+\lambda_o}\frac{e^{jk\tau/2\sin\phi_o}}{\mathcal{G}_{1-}^{odd}(\lambda)\mathcal{G}_{1-}^{odd}(\lambda_o)\mathcal{G}_{2+}^{odd}(\lambda)\mathcal{G}_{2+}^{odd}(\lambda_o)}$$
$$\cdot\left[Z_{odd}\left(\lambda_o^2\right)\frac{E_{odd}(\lambda)}{E_{odd}(-\lambda_o)}+\sum_{m=1}^{\widetilde{N}_{odd}-1}\sum_{n=0}^{\widetilde{N}_{odd}-1-m}a_{mn}(\lambda+\lambda_o)^m(\lambda\lambda_o)^n\right] \quad (29)$$

where we have assumed that $J_{odd}(x)\sim x^{S_{odd}}$ as $x\to 0$ with $0<S_{odd}<1$. In this, $\widetilde{N}_{odd}=int\{1/2(N_{odd}^1+N_{odd}^2+1)\}$, and a_{mn} are arbitrary constants as yet undetermined, and correspond to the coefficients of the polynomial resulting from the application of Liouville's theorem. The chosen symmetric form of this polynomial is not unique but will be found most useful later in constructing a reciprocal form for $P_{odd}(\lambda)$. Also, $G_{1+}(\lambda)$ are Wiener-Hopf split function regular in the upper (+) or lower (-) half of the λ-plane and satisfy the relation

$$G_1(\lambda^2)=G_{1+}(\lambda)G_{1-}(\lambda) \quad (30)$$

(see Appendix). Similarly, $G_{2\pm}(\lambda)$ are the corresponding split functions associated with $G_2(\lambda^2)$. Finally, $E_{odd}(\lambda)$ is some entire function behaving no worse than $|\lambda|^{(N_{odd}^1+N_{odd}^2)/2-S_{odd}}$ and can take any of the forms

$$E_{odd}(\lambda) = \begin{cases} Z_{odd}(-\lambda\lambda_o) & \text{or} \\ Z_{odd}^-(\lambda) & \text{or} \\ Z_{odd}^+(\lambda) & \end{cases} \quad (31)$$

where $Z^{\pm}(\lambda)$ are again upper and lower functions satisfying the relation

$$Z(\lambda^2)=Z^+(\lambda)Z^-(\lambda) \quad (32)$$

Following a similar procedure we obtain $P_{even}(\lambda)$ as

$$P_{even}(\lambda) = \frac{j}{2\pi}\frac{\sin\phi_o\sqrt{1-\lambda^2}}{\lambda+\lambda_o}\frac{e^{jk\tau/2\sin\phi_o}}{\mathcal{G}_{1-}^{even}(\lambda)\mathcal{G}_{1-}^{even}(\lambda_o)\mathcal{G}_{2+}^{even}(\lambda)\mathcal{G}_{2+}^{even}(\lambda_o)}$$
$$\cdot\left[Z_{even}\left(\lambda_o^2\right)\frac{E_{even}(\lambda)}{E_{even}(-\lambda_o)}+\sum_{m=1}^{\widetilde{N}_{even}-1}\sum_{n=0}^{\widetilde{N}_{even}-1-m}b_{mn}(\lambda+\lambda_o)^m(\lambda\lambda_o)^n\right] \quad (33)$$

with $E_{even}(\lambda)$, $\widetilde{N}_{even}$ and b_{mn} being the counterparts of $E_{odd}(\lambda)$, $\widetilde{N}_{odd}$ and a_{mn}, respectively. Taking into account the choices (31), we may substitute (29) and (33) into (14) and subsequently perform a steepest descent path evaluation to obtain for $\rho \to \infty$ (all surface wave contributions are neglected in this evaluation)

$$F(\rho,\phi) \sim [D_{odd}(\phi,\phi_o) + D_{even}(\phi,\phi_o)] \frac{e^{-jk\rho}}{\sqrt{k\rho/2\pi}} \tag{34}$$

where (ρ,ϕ) are the usual cylindrical coordinates and $D_{odd}(\phi,\phi_o)+D_{even}(\phi,\phi_o)$ is the far zone diffraction coefficient symmetric with respect to ϕ and ϕ_o. We have

$$\begin{aligned} D_{odd}(\phi,\phi_o) &= -\frac{e^{-j\pi/4}}{2\pi}\frac{\sin\phi_o \sin\phi}{\cos\phi+\cos\phi_o} \\ &\cdot \frac{e^{jk\tau/2(\sin\phi_o+|\sin\phi|)}}{\mathcal{G}_{1-}^{odd}(\cos\phi)\,\mathcal{G}_{1-}^{odd}(\cos\phi_o)\,\mathcal{G}_{2+}^{odd}(\cos\phi)\,\mathcal{G}_{2+}^{odd}(\cos\phi_o)} \\ &\cdot \left[\tilde{Z}_{odd}(\cos\phi,\cos\phi_o) + \sum_{m=1}^{\widetilde{N}_{odd}-1}\sum_{n=0}^{\widetilde{N}_{odd}-1-m} a_{mn} \right. \\ &\left. \cdot (\cos\phi+\cos\phi_o)^m (\cos\phi\cos\phi_o)^n \right] \end{aligned} \tag{35}$$

$$\begin{aligned} D_{even}(\phi,\phi_o) &= -\frac{e^{-j\pi/4}}{2\pi}\frac{\sin\phi_o|\sin\phi|}{\cos\phi+\cos\phi_o} \\ &\cdot \frac{e^{jk\tau/2(\sin\phi_o+|\sin\phi|)}}{\mathcal{G}_{1-}^{even}(\cos\phi)\,\mathcal{G}_{1-}^{even}(\cos\phi_o)\,\mathcal{G}_{2+}^{even}(\cos\phi)\,\mathcal{G}_{2+}^{even}(\cos\phi_o)} \\ &\cdot \left[\tilde{Z}_{even}(\cos\phi,\cos\phi_o) + \sum_{m=1}^{\widetilde{N}_{even}-1}\sum_{n=0}^{\widetilde{N}_{even}-1-m} b_{mn} \right. \\ &\left. \cdot (\cos\phi+\cos\phi_o)^m (\cos\phi\cos\phi_o)^n \right] \end{aligned} \tag{36}$$

in which the functions $\tilde{Z}_{odd,even}(\cos\phi, \cos\phi_o)$ are given by (see (31))

$$\tilde{Z}_{odd}(\cos\phi, \cos\phi_o) = \begin{cases} Z_{odd}(-\cos\phi\cos\phi_o) & \text{or} \\ Z^{-}_{odd}(\cos\phi)\, Z^{-}_{odd}(\cos\phi_o) & \text{or} \\ Z^{+}_{odd}(\cos\phi)\, Z^{+}_{odd}(\cos\phi_o) \end{cases} \tag{37}$$

$$\tilde{Z}_{even}(\cos\phi, \cos\phi_o) = \begin{cases} Z_{even}(-\cos\phi\cos\phi_o) & \text{or} \\ Z^{-}_{even}(\cos\phi)\, Z^{-}_{even}(\cos\phi_o) & \text{or} \\ Z^{+}_{even}(\cos\phi)\, Z^{+}_{even}(\cos\phi_o) \end{cases} \tag{38}$$

Because the above three choices for $\tilde{Z}_{odd}$ and $\tilde{Z}_{even}$ differ only by terms of the form $(\cos\phi + \cos\phi_o)^m (\cos\phi\cos\phi_o)^n$, it is immaterial which of them we choose, although one of the choices may likely lead to a more compact representation. Nevertheless, regardless of the choice of $\tilde{Z}_{odd}$ and $\tilde{Z}_{even}$, one is still faced with the determination of the unknown constants a_{mn} and b_{mn} in (35) and (36), repectively. These are a manifestation of the non-uniqueness of the finite-order GSTC sheet model employed herein, and their explicit determination requires the introduction of additional constraints pertaining to the physics of the problem. Before we consider their determination for the general case, we first look at a specific example, that of diffraction by a thin single layer junction.

4 Diffraction by Thin Single Layer Discontinuous Slabs

The diffraction coefficient given by (35) and (36) is very general and can model a wide variety of geometries. To check its validity, display its versatility, and assess the relative importance of the unknown constants, we consider the thin material-to-material junction of thickness $2w$ as shown in Figure 4. The slab will be modelled by a sheet of thickness $2(w - w_s)$ and with a proper choice of the material parameters this geometry can reduce to junctions whose diffracted field is available, thus, permitting some validation of our solution.

If the left hand side of the slab, in addition to being thin, is also associated with low index of refraction, it may be modeled by a low contrast GSTC sheet. Thus, an $O(w^1, w_s^1)$ approximation with terms of $O(w_s w)$ neglected is sufficient for the representation of the operators or polynomials

$\mathcal{U}^1_{ij}$. In particular, we have

$$\begin{aligned}
\mathcal{U}^1_{11}\left(-\partial x^2/k^2\right) &= 1 \\
\mathcal{U}^1_{12}\left(-\partial x^2/k^2\right) &= jk\left(u_1 w - w_s\right) \\
\mathcal{U}^1_{21}\left(-\partial x^2/k^2\right) &= jk\left(\frac{w\epsilon_1\mu_1}{u_1} - w_s\right) + \frac{j}{k}\left(\frac{w}{u_1} - w_s\right)\partial x^2 \\
\mathcal{U}^1_{22}\left(-\partial x^2/k^2\right) &= 1
\end{aligned} \tag{39}$$

where ϵ_1 and μ_1 are the relative permittivity and permeability of the left hand slab, respectively, and

$$u_1 = \begin{cases} \mu_1, & E_z \text{ polarization} \\ \epsilon_1 & H_z \text{ polarization} \end{cases} . \tag{40}$$

Also, when $w_s = w$, these are simply the transition conditions derived first by Weinstein [5] and later by Senior and Volakis [6]. The corresponding polynomials to be employed in (23) - (28) are given by

$$\begin{aligned}
&\mathcal{U}^1_{11}\left(-\cos\phi\cos\phi_o\right) = 1 \\
&\mathcal{U}^1_{12}\left(-\cos\phi\cos\phi_o\right) = jk\left(u_1 w - w_s\right) \\
&\mathcal{U}^1_{21}\left(-\cos\phi\cos\phi_o\right) = jk\left(\frac{w\epsilon_1\mu_1}{u_1} - w_s\right) + jk\left(\frac{w}{u_1} - w_s\right)\cos\phi\cos\phi_o \\
&\mathcal{U}^1_{22}\left(-\cos\phi\cos\phi_o\right) = 1
\end{aligned} \tag{41}$$

Incorporating these into (35) and (36) and setting

$$\tilde{Z}_{odd}\left(\cos\phi, \cos\phi_o\right) = Z_{odd}\left(-\cos\phi\cos\phi_o\right) \tag{42}$$

$$\tilde{Z}_{even}\left(\cos\phi, \cos\phi_o\right) = Z_{even}\left(-\cos\phi\cos\phi_o\right) \tag{43}$$

yields

$$\begin{aligned}
D_{odd}\left(\phi, \phi_o\right) &= -\frac{e^{-j\pi/4}}{2\pi}\frac{\sin\phi_o\sin\phi}{\cos\phi + \cos\phi_o}e^{jk\tau/2\left(\sin\phi_o + |\sin\phi|\right)} \\
&\cdot \frac{\mathcal{U}^2_{12}\left(-\cos\phi\cos\phi_o\right) - jk\left(u_1 w - w_s\right)\mathcal{U}^2_{11}\left(-\cos\phi\cos\phi_o\right)}{M_-\left(\cos\phi; \gamma^{odd,1}\right) M_-\left(\cos\phi_o; \gamma^{odd,1}\right) \mathcal{G}^{odd}_{2+}\left(\cos\phi\right) \mathcal{G}^{odd}_{2+}\left(\cos\phi_o\right)}
\end{aligned} \tag{44}$$

$$D_{even}(\phi,\phi_o) = -\frac{e^{-j\pi/4}}{2\pi}\frac{\sin\phi_o|\sin\phi|}{\cos\phi+\cos\phi_o}e^{jk\tau/2(\sin\phi_o+|\sin\phi|)}$$

$$\cdot\left\{\frac{[\alpha_1+\alpha_2\cos\phi\cos\phi_o]\mathcal{U}_{22}^2(-\cos\phi\cos\phi_o)-\mathcal{U}_{21}^2(-\cos\phi\cos\phi_o)}{\alpha_3\left[\prod_{m=1}^{2}M_-\left(\cos\phi;\gamma_m^{even,1}\right)M_-\left(\cos\phi_o;\gamma_m^{even,1}\right)\right]\mathcal{G}_{2+}^{even}(\cos\phi)\mathcal{G}_{2+}^{even}(\cos\phi_o)}\right.$$

$$\left.+\frac{b_{10}(\cos\phi+\cos\phi_o)}{\alpha_3\left[\prod_{m=1}^{2}M_-\left(\cos\phi;\gamma_m^{even,1}\right)M_-\left(\cos\varphi_o;\gamma_m^{even,1}\right)\right]\mathcal{G}_{2+}^{even}(\cos\phi)\mathcal{G}_{2+}^{even}(\cos\phi_o)}\right\} \qquad (45)$$

where the split function $M_-(\cos\phi;\gamma)$ is given in the Appendix,

$$\begin{aligned}\alpha_1 &= jk\left(\frac{w\epsilon_1\mu_1}{u_1}-w_s\right)\\ \alpha_2 &= jk\left(\frac{w}{u_1}-w_s\right)\\ \alpha_3 &= \frac{jkw}{u_1}(\epsilon_1\mu_1-1)\end{aligned} \qquad (46)$$

and

$$\begin{aligned}\gamma^{odd,1} &= \frac{-j}{k(u_1w-w_s)}\\ \gamma_{1,2}^{even,1} &= \frac{u_1\pm\sqrt{u_1^2+4k^2w(\epsilon_1\mu_1-1)(w-u_1w_s)}}{2jk(w-w_su_1)}\end{aligned} \qquad (47)$$

with $\gamma^{odd\ or\ even}$ are associated with possible surface wave poles. To complete the definition of (44) and (45), the functions associated with the right hand side properties of the slab (i.e. those functions with the superscript 2) must be specified and Tables 1 and 2 provide explicit expressions for the functions $\mathcal{U}_{ij}^2(-\cos\phi\cos\phi_o)$, $\mathcal{G}_{2+}^{odd}(\cos\phi)\,\mathcal{G}_{2+}^{odd}(\cos\phi_o)$ and $\mathcal{G}_{2+}^{even}(\cos\phi)\ \mathcal{G}_{2+}^{even}(\cos\phi_o)$ terms. By edge condition considerations, all of the constants a_{mn} and b_{mn} have been set to zero except b_{10} appearing in the definition of D_{even}, which is non-zero unless the right hand side slab is a PEC/PMC under an E_z/H_z excitation (see Table 2).

By invoking image theory the diffraction coefficient for the grounded metal- dielectric join, shown in Figure 5 is given by

$$D_{rs}(\cos\phi,\cos\phi_o) = 2D_{even}(\cos\phi,\cos\phi_o) \qquad (48)$$

The GSTC or GIBC model for this structure cannot dsicriminate whether the stub at the junction is a perfect electric conductor (PEC) or perfect magnetic conductor (PMC). This information can only be carried by the constant b_{10} and its determination must somehow involve the properties of the junction across its thickness as discussed in a subsequent section. However, since the diffraction coefficient for the junction in Figure 5 is already available [15], b_{10} can be identified. Upon setting $w_s = 0$, we find

$$b_{10}^{\text{no stub}} = jkw\sqrt{\frac{\mu_1}{\epsilon_1}} \tag{49}$$

$$b_{10}^{\text{pec stub}} = \frac{jkw\sqrt{\frac{\mu_1}{\epsilon_1}}}{\frac{jkw}{4\epsilon_1}\left(\sqrt{\epsilon_1\mu_1}-1\right)\left[M_-\left(\sqrt{\epsilon_1\mu_1},\gamma_1^{even,1}\right)M_-\left(\sqrt{\epsilon_1\mu_1},\gamma_2^{even,1}\right)\right]^2+\frac{1}{2}} \tag{50}$$

$$b_{10}^{\text{pmc stub}} = \frac{jkw\sqrt{\frac{\mu_1}{\epsilon_1}}}{\frac{jkw}{4\epsilon_1}\left(\sqrt{\epsilon_1\mu_1}-1\right)\left[M_-\left(\sqrt{\epsilon_1\mu_1},\gamma_1^{even,1}\right)M_-\left(\sqrt{\epsilon_1\mu_1},\gamma_2^{even,1}\right)\right]^2-\frac{1}{2}} \tag{51}$$

This comparison clearly demonstrates the importance of the constant b_{10} and by referring to Figure 6 we observe that it plays a major role in the computation of the diffracted field.

5 Modal Decomposition of the Symmetric Slab Fields

A general approach for determining the solution constants is to enforce tangential field continuity accross the junction. This, of course, demands a knowledge of the fields internal to the discontinuous slab, which are not readily available when a GSTC simulation is employed. The Weiner-Hopf (or dual integral equations) solution in conjunction with the GSTC provides only the fields external to the slab, and this section deals with the determination of the internal fields from the external ones.

A modal representation of the internal field is first proposed comprised of discrete and continuous spectral components. This representation is compatible with that given by Shevchenko [16] whose eigenfunctions are chosen to satisfy field continuity across all layer interfaces including the air-dielectric interface. Consequently, the representation is valid inside and

outside the dielectric once the coefficients of the modal representation are determined. This is accomplished by recasting the Weiner-Hopf or dual integral equation solution given earlier (see (13), (14), (29) and (33)) in a form compatible with the proposed modal representation, thus permitting the identification of the modal or eigenfunction coefficients. These will, of course, be in terms of the unknown constants appearing in the Weiner-Hopf solution and the enforcement of field continuity across the junction leads to a linear system of equations to be solved for the constants as described in the next section.

For the symmetric slab in Figure 2, the total field may be decomposed into its odd and even components. Specifically we write

$$F(x,y) = \begin{cases} F^{1,odd}(x,y) + F^{1,even}(x,y) & x < 0 \\ \\ F^{2,odd}(x,y) + F^{2,even}(x,y) & x > 0 \end{cases} \tag{52}$$

where $F^{odd}(x,y) = -F^{odd}(x,-y)$ and $F^{even}(x,y) = F^{even}(x,-y)$. Following [16], the odd and even fields interior and exterior to the slab may be expanded into discrete and continuous eigenmodes as

$$\begin{aligned} F^{1,odd}(x,y) &= \sum_{m=1}^{N_{go}} A_m^{1,odd} \Psi^{1,odd}\left(\left(\lambda_m^{1,go}\right)^2, y\right) e^{-jkx\lambda_m^{1,go}} \\ &\quad + \sum_{m=1}^{N_{sw}^{1,odd}} B_m^{1,odd} \Phi_m^{1,odd}(y)\, e^{-jkx\lambda_m^{1,odd}} \\ &\quad + \int_0^{\infty} C^{1,odd}(\beta)\, \Psi^{1,odd}\left(\lambda^2, y\right) e^{-jkx\lambda} d\beta \end{aligned} \tag{53}$$

$$\begin{aligned} F^{1,even}(x,y) &= \sum_{m=1}^{N_{go}} A_m^{1,even} \Psi^{1,even}\left(\left(\lambda_m^{1,go}\right)^2, y\right) e^{-jkx\lambda_m^{1,go}} \\ &\quad + \sum_{m=1}^{N_{sw}^{1,even}} B_m^{1,even} \Phi_m^{1,even}(y)\, e^{-jkx\lambda_m^{1,even}} \\ &\quad + \int_0^{\infty} C^{1,even}(\beta)\, \Psi^{1,even}\left(\lambda^2, y\right) e^{-jkx\lambda} d\beta \end{aligned} \tag{54}$$

$$F^{2,odd}(x,y) = \sum_{m=1}^{N_{go}} A_m^{2,odd} \Psi^{2,odd}\left(\left(\lambda_m^{2,go}\right)^2, y\right) e^{-jkx\lambda_m^{2,go}}$$

$$+\sum_{m=1}^{N_{sw}^{2,odd}} B_m^{2,odd}\Phi_m^{2,odd}(y)\,e^{-jkx\lambda_m^{2,odd}} + \int_0^{\infty} C^{2,odd}(\beta)\,\Psi^{2,odd}\left(\lambda^2,y\right)e^{-jkx\lambda}d\beta \qquad (55)$$

$$F^{2,even}(x,y) = \sum_{m=1}^{N_{go}} A_m^{2,even}\Psi^{2,even}\left(\left(\lambda_m^{2,go}\right)^2,y\right)e^{-jkx\lambda_m^{23,go}} + \sum_{m=1}^{N_{sw}^{2,even}} B_m^{2,even}\Phi_m^{2,even}(y)\,e^{-jkx\lambda_m^{2,even}} + \int_0^{\infty} C^{2,even}(\beta)\,\Psi^{2,even}\left(\lambda^2,y\right)e^{-jkx\lambda}d\beta \qquad (56)$$

where $Im\{\lambda_m^{odd,even}\} < 0$ and $\lambda = \sqrt{1-\beta^2}$, with the branch of the square root chosen so that $Im\{\sqrt{1-\beta^2}\} < 0$. In (53)- (56), $\Psi^{odd,even}$ are referred to as the cross section functions corresponding to the continuous modal fields whereas $\Phi_m^{odd,even}$ are the corresponding cross section functions for the discrete modal fields associated with the surface waves. The cross section function associated with the geometrical optics fields is also $\Psi^{odd,even}$ evaluated at $\lambda = \lambda_m^{go}$, where $\lambda_m^{go}$is a parameter to be determined later. As can be observed from (53) - (56), the cross section functions specify the field behavior in the plane normal to the slab, and hence all information pertaining to the fields interior to the slab are embedded into these functions. They will be chosen to satisfy the orthogonality relations (where $u(y)$ is $\mu(y)$ or $\epsilon(y)$ for E_z or H_z polarization, respectively)

$$\int_{-\infty}^{\infty} \frac{\Psi(\lambda^2,y)\,\Psi\left(\tilde{\lambda}^2,y\right)}{u(y)}dy = 0 \quad \text{for } \lambda \neq \tilde{\lambda} \qquad (57)$$

$$\int_{-\infty}^{\infty} \frac{\Phi_m(y)\,\Psi(\lambda^2,y)}{u(y)}dy = 0 \qquad (58)$$

and thus each discrete eigenmode $\Phi_m(y)\,e^{-jkx\lambda}$ and each continuous eigenmode $\Psi(\lambda^2,y)\,e^{-jkx\lambda}$ must satisfy the wave equation. Additional details pertaining to the cross section functions are given in [16].

Exterior Cross Section Functions

To compute the cross section functions in the exterior slab region $|y| > \tau/2$, we recall that in accordance with the slab simulation based on the generalized sheet transition conditions (GSTCs), the external fields satisfy the conditions (10) and (11). Because of the orthogonality relations (57) and (58), each of the cross section functions $\Psi(\lambda^2, y)$ and $\Phi_m(y)$ must then satisfy their respective odd or even GSTC. In view of this we set

$$\begin{aligned}\Psi^{p,odd}\left(\lambda^2, y\right) &= \frac{|y|}{y}\left\{\mathcal{U}_{11}^{p}\left(\lambda^2\right) j\frac{\sin\left[k\left(|y|-\tau/2\right)\sqrt{1-\lambda^2}\right]}{\sqrt{1-\lambda^2}}\right. \\ &\quad \left.+\mathcal{U}_{12}^{p}\left(\lambda^2\right)\cos\left[k\left(|y|-\tau/2\right)\sqrt{1-\lambda^2}\right]\right\} \\ &= \frac{|y|}{y}\left\{\mathcal{U}_{11}^{p}\left(\lambda^2\right)\tilde{q}_{12}(1,1,|y|-\tau/2,\lambda^2)\right. \\ &\quad \left.+\mathcal{U}_{12}^{p}\left(\lambda^2\right)\tilde{q}_{22}(1,1,|y|-\tau/2,\lambda^2)\right\} \qquad (59)\end{aligned}$$

$$\begin{aligned}\Psi^{p,even}\left(\lambda^2, y\right) &= \left\{\mathcal{U}_{21}^{p}\left(\lambda^2\right) j\frac{\sin\left[k\left(|y|-\tau/2\right)\sqrt{1-\lambda^2}\right]}{\sqrt{1-\lambda^2}}\right. \\ &\quad \left.+\mathcal{U}_{22}^{p}\left(\lambda^2\right)\cos\left[k\left(|y|-\tau/2\right)\sqrt{1-\lambda^2}\right]\right\} \\ &= \left\{\mathcal{U}_{21}^{p}\left(\lambda^2\right)\tilde{q}_{12}(1,1,|y|-\tau/2,\lambda^2)\right. \\ &\quad \left.+\mathcal{U}_{22}^{p}\left(\lambda^2\right)\tilde{q}_{22}(1,1,|y|-\tau/2,\lambda^2)\right\} \qquad (60)\end{aligned}$$

where $\tilde{q}_{ij}$ represents the infinite order form of the q_{ij} layer operators given in [10]. Once each of the modes comprising (53) through (56) is substituted into (10) or (11), the differentiation implied by $-\partial x^2/k^2$ reduces to a multiplication by λ^2 and the above $\Psi^{p,odd}$ and $\Psi^{p,even}$ are then readily shown to satisfy the associated GSTC. It can also be shown that these satisfy the orthogonality conditions (57) and (58).

A customary representation for the surface wave cross section functions is

$$\Phi_m^{p,odd}(y) = \frac{|y|}{y}e^{-jk(|y|-\tau/2)\sqrt{1-\left(\lambda_m^{p,odd}\right)^2}} \quad ;|y| > \tau/2 \qquad (61)$$

$$\Phi_m^{p,even}(y) = e^{-jk(|y|-\tau/2)\sqrt{1-\left(\lambda_m^{p,even}\right)^2}} \quad ;|y| > \tau/2 \qquad (62)$$

where $\lambda_m^{p,even,odd}$ must now be chosen so that they satisfy their associated GSTC. By substituting (61) and (62) into (10) and (11), we find that $\lambda_m^{odd,even}$ must satisfy the polynomial equations

$$\sqrt{1-\left(\lambda_m^{p,odd}\right)^2}\mathcal{U}_{12}^p\left(\left[\lambda_m^{p,odd}\right]^2\right)+\mathcal{U}_{11}^p\left(\left[\lambda_m^{p,odd}\right]^2\right) = 0 \tag{63}$$

$$\sqrt{1-(\lambda_m^{p,even})^2}\mathcal{U}_{22}^p\left([\lambda_m^{p,even}]^2\right)+\mathcal{U}_{21}^p\left([\lambda_m^{p,even}]^2\right) = 0 \tag{64}$$

and can be also identified as the poles of the slab plane wave reflection coefficient. We further note that

$$\Phi_m^{p,odd}(y) = \frac{\Psi^{p,odd}\left(\left[\lambda_m^{p,odd}\right]^2,y\right)}{\mathcal{U}_{12}^p\left(\left[\lambda_m^{p,odd}\right]^2\right)};\quad |y|>\tau/2 \tag{65}$$

$$\Phi_m^{p,even}(y) = \frac{\Psi^{p,even}\left([\lambda_m^{p,even}]^2,y\right)}{\mathcal{U}_{22}^p\left([\lambda_m^{p,even}]^2\right)};\quad |y|>\tau/2 \tag{66}$$

implying that for a multilayer slab the cross section functions associated with the discrete and continuous eigenmodes are of the same generic form given by (59) and (60).

Interior Cross Section Functions

We consider now the determination of the cross section functions for the region interior to the slab (i.e. in the region $|y|<\tau/2$). For simplicity let us first assume a single layer slab of thickness $\tau=\tau_1$, whose upper face is located at $y=-\tau_1/2$. In accordance with the preceeding, the cross section functions associated with the external fields are given by

$$\begin{aligned}\Psi^{p,odd}\left(\lambda^2,y\right) &= \frac{|y|}{y}\left\{q_{11}\left(u_1^p,\kappa_1^p,\tau_1^p,\lambda^2\right)\tilde{q}_{12}(1,1,|y|-\tau_1/2,\lambda^2)\right.\\ &\left.+\,q_{12}\left(u_1^p,\kappa_1^p,\tau_1^p,\lambda^2\right)\tilde{q}_{22}(1,1,|y|-\tau_1/2,\lambda^2)\right\};\quad |y|>\tau_1/2\end{aligned} \tag{67}$$

$$\begin{aligned}\Psi^{p,even}\left(\lambda^2,y\right) &= \left\{q_{21}\left(u_1^p,\kappa_1^p,\tau_1^p,\lambda^2\right)\tilde{q}_{12}(1,1,|y|-\tau_1/2,\lambda^2)\right.\\ &\left.+q_{22}\left(u_1^p,\kappa_1^p,\tau_1^p,\lambda^2\right)\tilde{q}_{22}(1,1,|y|-\tau_1/2,\lambda^2)\right\};\quad |y|>\tau_1/2\end{aligned} \tag{68}$$

obtained by setting $\mathcal{U}_{ij}^{p}(\lambda^2) = q_{ij}(u_1^p, \kappa_1^p, \tau_1^p, \lambda^2)$ in (59) and (60). These are orthogonal functions and each must, therefore, satisfy the continuity conditions

$$\Psi^{p,odd}\left(\lambda^2, \tau_1^-\right) = \Psi^{p,odd}\left(\lambda^2, \tau_1^+\right) \tag{69}$$

$$\frac{1}{u_1}\partial_y \Psi^{p,odd}\left(\lambda^2, \tau_1^-\right) = \partial_y \Psi^{p,odd}\left(\lambda^2, \tau_1^+\right) \tag{70}$$

$$\Psi^{p,even}\left(\lambda^2, \tau_1^-\right) = \Psi^{p,even}\left(\lambda^2, \tau_1^+\right) \tag{71}$$

$$\frac{1}{u_1}\partial_y \Psi^{p,even}\left(\lambda^2, \tau_1^-\right) = \partial_y \Psi^{p,even}\left(\lambda^2, \tau_1^+\right) \tag{72}$$

with similar conditions on $\Phi_m^{odd,even}(y)$. It is now straightforward to deduce that possible cross section functions satisfying (69) - (72) are of the form

$$\Psi^{p,odd}\left(\lambda^2, y\right) = \frac{|y|}{y} q_{12}(u_1^p, \kappa_1^p, |y|, \lambda^2) \tag{73}$$

$$\Psi^{p,even}\left(\lambda^2, y\right) = q_{22}(u_1^p, \kappa_1^p, |y|, \lambda^2) \tag{74}$$

for $|y| < \tau/2$. Also, in view of (69) - (72), the cross section functions for the surface wave modes remain as given in (65) - (66), provided (73) and (74) are used in place of $\Psi^{odd,even}$.

For the general case of a multilayer slab, it is necessary that each of the internal cross sections functions satisfy the continuity conditions at all layer interfaces comprising the slab. In this case we find that

$$\Psi^{p,odd}\left(\lambda^2, y\right) = \frac{|y|}{y} \begin{cases} \mathcal{U}_{11}^{p}(\lambda^2)\,\tilde{q}_{12}(1,1,|y|-\tau/2,\lambda^2) \\ \quad +\mathcal{U}_{12}^{p}(\lambda^2)\,\tilde{q}_{22}(1,1,|y|-\tau/2,\lambda^2); \\ \qquad\qquad |y| > \tau/2 \\ \mathcal{P}_{11}^{l,p}(\lambda^2)\,q_{12}(u_l^p, \kappa_l^p, |y|-y_{l-1}, \lambda^2) \\ \quad +\mathcal{P}_{12}^{l,p}(\lambda^2)\,q_{22}(u_l^p, \kappa_l^p, |y|-y_{l-1}, \lambda^2); \\ \qquad\qquad y_l > |y| > y_{l-1} \\ q_{12}(u_1^p, \kappa_1^p, |y|, \lambda^2); \quad |y| < y_1 \end{cases} \tag{75}$$

$$\Psi^{p,even}\left(\lambda^2,y\right) = \begin{cases} \mathcal{U}_{21}^{p}\left(\lambda^2\right)\tilde{q}_{12}(1,1,|y|-\tau/2,\lambda^2) \\ \quad +\mathcal{U}_{22}^{p}\left(\lambda^2\right)\tilde{q}_{22}(1,1,|y|-\tau/2,\lambda^2); \\ \qquad\qquad |y|>\tau/2 \\ \mathcal{P}_{21}^{l,p}\left(\lambda^2\right)q_{12}(u_l^p,\kappa_l^p,|y|-y_{l-1},\lambda^2) \\ \quad +\mathcal{P}_{22}^{l,p}\left(\lambda^2\right)q_{22}(u_l^p,\kappa_l^p,|y|-y_{l-1},\lambda^2); \\ \qquad\qquad y_l>|y|>y_{l-1} \\ q_{22}(u_1^p,\kappa_1^p,|y|,\lambda^2); \quad |y|<y_1 \end{cases} \tag{76}$$

where

$$\begin{pmatrix} \mathcal{P}_{11}^{l,p}\left(-\frac{\partial x^2}{k^2}\right) & \mathcal{P}_{12}^{l,p}\left(-\frac{\partial x^2}{k^2}\right) \\ \mathcal{P}_{21}^{l,p}\left(-\frac{\partial x^2}{k^2}\right) & \mathcal{P}_{22}^{l,p}\left(-\frac{\partial x^2}{k^2}\right) \end{pmatrix} = \prod_{m=1}^{l} \cdot \begin{pmatrix} q_{11}(u_m^p,\kappa_m^p,\tau_m^p,-\frac{\partial x^2}{k^2}) & q_{12}(u_m^p,\kappa_m^p,\tau_m^p,-\frac{\partial x^2}{k^2}) \\ q_{21}(u_m^p,\kappa_m^p,\tau_m^p,-\frac{\partial x^2}{k^2}) & q_{22}(u_m^p,\kappa_m^p,\tau_m^p,-\frac{\partial x^2}{k^2}) \end{pmatrix} \tag{77}$$

When these are used in (53) - (56) in conjunction with (65) and (66) we have a complete field representation for all x.

6 Recasting of the Dual Integral Equation Solution for a Material Junction

The expressions (53) - (56) can be used to represent the fields interior and exterior to the slab. It remains to find the coefficients of these expansions and to do this we must first rewrite $F(x,y)$ in a form compatible with (53) - (56). That is, we need to identify from (13) and (14) the discrete and continuous spectral components. The discrete portion of the spectrum is, of course, comprised of the geometrical optics and the surface wave fields. These can be identified by detouring the integration path in (14) as shown in Figure 7. In particular, for $x<0$ the integration path may be deformed to one over the branch cut in the upper half of the λ plane, capturing any surface wave poles attributed to the zeros of $\mathcal{G}_{1-}^{odd}(\lambda)$ and $\mathcal{G}_{1-}^{even}(\lambda)$. Similarly, for $x>0$, the integration path may be deformed to one over the branch cut in the lower half of the λ plane causing the capture of the geometrical optics pole at $\lambda=-\lambda_o$ in addition to any surface wave poles attributed to the zeros of $\mathcal{G}_{2+}^{odd}(\lambda)$ and $\mathcal{G}_{2+}^{even}(\lambda)$.

Through the above deformation of the integration paths in (14) we obtain

$$F^{odd}(x,y) = \begin{cases} F_{go}^{1,odd}(x,y) + F_{sw}^{1,odd}(x,y) + F_{diff}^{1,odd}(x,y) & x < 0 \\ F_{go}^{2,odd}(x,y) + F_{sw}^{2,odd}(x,y) + F_{diff}^{2,odd}(x,y) & x > 0 \end{cases} \tag{78}$$

$$F^{even}(x,y) = \begin{cases} F_{go}^{1,even}(x,y) + F_{sw}^{1,even}(x,y) + F_{diff}^{1,even}(x,y) & x < 0 \\ F_{go}^{2,even}(x,y) + F_{sw}^{2,even}(x,y) + F_{diff}^{2,even}(x,y) & x > 0 \end{cases} \tag{79}$$

where the components F_{go}, F_{sw}, F_{diff} denote the geometrical optics, surface wave, and branch cut (or diffraction) contributions to the total fields.

After some manipulation we find

$$F_{go}^{1,odd}(x,y) = A_1^{1,odd}(\lambda_o)\,\Psi^{1,odd}\left(\lambda_o^2, y\right) e^{jkx\cos\phi_o} \tag{80}$$

$$F_{go}^{2,odd}(x,y) = A_1^{2,odd}(\lambda_o)\,\Psi^{2,odd}\left(\lambda_o^2, y\right) e^{jkx\cos\phi_o} \tag{81}$$

$$F_{go}^{1,even}(x,y) = A_1^{1,even}(\lambda_o)\,\Psi^{1,even}\left(\lambda_o^2, y\right) e^{jkx\cos\phi_o} \tag{82}$$

$$F_{go}^{2,even}(x,y) = A_1^{2,even}(\lambda_o)\,\Psi^{2,even}\left(\lambda_o^2, y\right) e^{jkx\cos\phi_o} \tag{83}$$

where the A expansion coefficients are identified as

$$A_1^{1,odd}(\lambda_o) = \frac{\sin\phi_o e^{jk\tau/2\sin\phi_o}}{\mathcal{G}_1^{odd}(\lambda_o^2)} \tag{84}$$

$$A_1^{2,odd}(\lambda_o) = \frac{\sin\phi_o e^{jk\tau/2\sin\phi_o}}{\mathcal{G}_2^{odd}(\lambda_o^2)} \tag{85}$$

$$A_1^{1,even}(\lambda_o) = \frac{\sin\phi_o e^{jk\tau/2\sin\phi_o}}{\mathcal{G}_1^{even}(\lambda_o^2)} \tag{86}$$

$$A_1^{2,even}(\lambda_o) = \frac{\sin\phi_o e^{jk\tau/2\sin\phi_o}}{\mathcal{G}_2^{even}(\lambda_o^2)} \tag{87}$$

For the B coefficients, we have

$$F_{sw}^{1,odd}(x,y) = \sum_{l=1}^{N_{sw}^{1,odd}} B_l^{1,odd}(\lambda_o)\left[Z_{odd}\left(-\lambda_o\lambda_l^{1,odd}\right)\right.$$

$$+\sum_{m=1}^{\widetilde{N}_{odd}-1}\sum_{n=0}^{\widetilde{N}_{odd}-1-m} a_{mn}\left(\lambda_l^{1,odd}+\lambda_o\right)^m\left(\lambda_l^{1,odd}\lambda_o\right)^n\Bigg]$$
$$\cdot\,\Psi^{1,odd}\left(\left[\lambda_l^{1,odd}\right]^2,y\right)e^{-jkx\lambda_l^{1,odd}} \tag{88}$$

$$F_{sw}^{1,even}(x,y) = \sum_{l=1}^{N_{sw}^{1,even}} B_l^{1,even}(\lambda_o)\Bigg[Z_{odd}\left(-\lambda_o\lambda_l^{1,even}\right)$$
$$+\sum_{m=1}^{\widetilde{N}_{even}-1}\sum_{n=0}^{\widetilde{N}_{even}-1-m} b_{mn}\left(\lambda_l^{1,even}+\lambda_o\right)^m\left(\lambda_l^{1,even}\lambda_o\right)^n\Bigg]$$
$$\cdot\,\Psi^{1,even}\left(\left[\lambda_l^{1,even}\right]^2,y\right)e^{-jkx\lambda_l^{1,even}} \tag{89}$$

with

$$B_l^{1,odd}(\lambda_o) = \frac{-\sin\phi_o}{\lambda_l^{1,odd}+\lambda_o}$$
$$\cdot\,\frac{e^{jk\tau/2\sin\phi_o}}{\left[\frac{\partial\mathcal{G}_{1-}^{odd}(\lambda)}{\partial\lambda}\right]_{\lambda=\lambda_l^{1,odd}}\mathcal{G}_{1-}^{odd}(\lambda_o)\,\mathcal{G}_{2+}^{odd}\left(\lambda_l^{1,odd}\right)\mathcal{G}_{2+}^{odd}(\lambda_o)} \tag{90}$$

$$B_l^{1,even}(\lambda_o) = \frac{-\sin\phi_o}{\lambda_l^{1,even}+\lambda_o}$$
$$\cdot\,\frac{e^{jk\tau/2\sin\phi_o}}{\left[\frac{\partial\mathcal{G}_{1-}^{even}(\lambda)}{\partial\lambda}\right]_{\lambda=\lambda_l^{1,even}}\mathcal{G}_{1-}^{even}(\lambda_o)\,\mathcal{G}_{2+}^{even}\left(\lambda_l^{1,even}\right)\mathcal{G}_{2+}^{even}(\lambda_o)} \tag{91}$$

The expressions for $F_{sw}^{2,odd}(x,y)$ and $F_{sw}^{2,even}(x,y)$ parallel those in (86) and (87).

To obtain the C coefficient we express $F_{diff}^{1,odd}$ as

$$F_{diff}^{1,odd}(x,y) = \frac{y}{|y|}\int_{-\infty}^{\infty}\frac{j}{2\pi}\frac{-\beta\sqrt{1-\lambda_o^2}}{\sqrt{1-\beta^2}\left(\sqrt{1-\beta^2}+\lambda_o\right)}$$
$$\cdot\,\frac{e^{jk\tau/2\left(\sqrt{1-\lambda_o^2}+\beta\right)}e^{-jk|y|\beta}e^{-jkx\sqrt{1-\beta^2}}}{\mathcal{G}_{1-}^{odd}\left(\sqrt{1-\beta^2}+\delta\frac{\beta}{|\beta|}\right)\mathcal{G}_{1-}^{odd}(\lambda_o)\,\mathcal{G}_{2+}^{odd}\left(\sqrt{1-\beta^2}\right)\mathcal{G}_{2+}^{odd}(\lambda_o)}$$

$$\cdot\left[Z_{odd}\left(-\lambda_o\sqrt{1-\beta^2}\right)+\sum_{m=1}^{\widetilde{N}_{odd}-1}\sum_{n=0}^{\widetilde{N}_{odd}-1-m}\right.$$

$$\left.\cdot a_{mn}\left(\lambda_o+\sqrt{1-\beta^2}\right)^m\left(\lambda_o\sqrt{1-\beta^2}\right)^n\right]d\beta \tag{92}$$

where the branch of the square root is chosen so that $I\!m(\sqrt{1-\beta^2})>0$ and δ is a vanishingly small positive number. By splitting the integral into its positive and negative portions, and employing some identities (92) becomes

$$F_{diff}^{1,odd}(x,y) = \int_0^\infty C^{1,odd}(\beta)\,\tilde{Z}_{odd}\left(\sqrt{1-\beta^2},\lambda_o\right)$$

$$\cdot\,\Psi^{1,odd}\left(1-\beta^2,y\right)e^{-jkx\sqrt{1-\beta^2}}d\beta \tag{93}$$

with the expansion coefficient $C^{1,odd}(\beta)$ given by

$$C^{1,odd}(\beta)=\frac{j}{\pi}\frac{\beta^2\sqrt{1-\lambda_o^2}}{\sqrt{1-\beta^2}\left(\sqrt{1-\beta^2}+\lambda_o\right)}$$

$$\cdot\frac{e^{jk\tau/2\sqrt{1-\lambda_o^2}}\mathcal{G}_{1+}^{odd}\left(\sqrt{1-\beta^2}\right)}{\mathcal{G}_{2+}^{odd}\left(\sqrt{1-\beta^2}\right)\mathcal{G}_{2+}^{odd}(\lambda_o)\,\mathcal{G}_{1-}^{odd}(\lambda_o)\left\{\left[\mathcal{U}_{11}^1(1-\beta^2)\right]^2-\beta^2\left[\mathcal{U}_{12}^1(1-\beta^2)\right]^2\right\}} \tag{94}$$

Similar expressions for $F_{diff}^{2,odd}(x,y)$, $F_{diff}^{1,even}(x,y)$ and $F_{diff}^{2,even}$ can be obtained in a parallel manner leading to the identification of the remaining C coefficient.

7 Determination of the Constants

To determine the constants a_{mn} and b_{mn}, we may now enforce the tangential field continuity conditions

$$F\left(x=0^-,y\right)=F\left(x=0^+,y\right);\quad |y|<\tau/2 \tag{95}$$

$$\frac{1}{u_1(y)}\partial xF(x,y)_{x=0^-}=\frac{1}{u_2(y)}\partial xF(x,y)_{x=0^+};\quad |y|<\tau/2 \tag{96}$$

with

$$u_{1,2}(y) = \begin{cases} \mu_{1,2}(y) & E_z\text{-pol} \\ \epsilon_{1,2}(y) & H_z\text{-pol} \end{cases} \tag{97}$$

and the subscripts 1 and 2 denoting quantities attributed to the left and right side of the slab. Substituting (79) - (79) into (95) and (96), we obtain

$$\begin{aligned} &F_{go}^{1,odd}\left(x=0^-,y\right)+F_{sw}^{1,odd}\left(x=0^-,y\right)+F_{diff}^{1,odd}\left(x=0^-,y\right) \\ &\quad=F_{go}^{2,odd}\left(x=0^+,y\right)+F_{sw}^{2,odd}\left(x=0^+,y\right)+F_{diff}^{2,odd}\left(x=0^+,y\right) \end{aligned} \tag{98}$$

$$\begin{aligned} &\frac{1}{u_1(y)}\partial x\left[F_{go}^{1,odd}(x,y)+F_{sw}^{1,odd}(x,y)+F_{diff}^{1,odd}(x,y)\right]_{x=0^-} \\ &\quad=\frac{1}{u_2(y)}\partial x\left[F_{go}^{2,odd}(x,y)+F_{sw}^{2,odd}(x,y)+F_{diff}^{2,odd}(x,y)\right]_{x=0^+} \end{aligned} \tag{99}$$

$$\begin{aligned} &F_{go}^{1,even}\left(x=0^-,y\right)+F_{sw}^{1,even}\left(x=0^-,y\right)+F_{diff}^{1,even}\left(x=0^-,y\right) \\ &\quad=F_{go}^{2,even}\left(x=0^+,y\right)+F_{sw}^{2,even}\left(x=0^+,y\right)+F_{diff}^{2,even}\left(x=0^+,y\right) \end{aligned} \tag{100}$$

$$\begin{aligned} &\frac{1}{u_1(y)}\partial x\left[F_{go}^{1,even}(x,y)+F_{sw}^{1,even}(x,y)+F_{diff}^{1,even}(x,y)\right]_{x=0^-} \\ &\quad=\frac{1}{u_2(y)}\partial x\left[F_{go}^{2,even}(x,y)+F_{sw}^{2,even}(x,y)+F_{diff}^{2,even}(x,y)\right]_{x=0^+} \end{aligned} \tag{101}$$

to be solved for all a_{mn} and b_{mn}. In particular, for an odd GSTC of $O(N_1^{odd})$ to the left and of $O(N_2^{odd})$ to the right of the discontinuity, the number of a_{mn} to be determined is equal to

$$\begin{aligned} N_a &= \frac{\widetilde{N}_{odd}\left(\widetilde{N}_{odd}-1\right)}{2} \\ &= \begin{cases} \frac{\left(N_{odd}^1+N_{odd}^2\right)\left(N_{odd}^1+N_{odd}^2-2\right)}{8}; & N_{odd}^1+N_{odd}^2 \text{ is even} \\ \frac{\left(N_{odd}^1+N_{odd}^2\right)^2-1}{8}; & N_{odd}^1+N_{odd}^2 \text{ is odd} \end{cases} \end{aligned} \tag{102}$$

To determine all a constants, (99) and/or (100) must then be enforced or sampled at a minimum of N_a points accross $|y| < \tau/2$ and $0 < \phi_o < \pi$. Similarly for an even GSTC of $O(N_1^{even})$ to the left and of $O(N_2^{even})$ to the

right of the discontinuity,

$$N_b = \frac{\widetilde{N}_{even}\left(\widetilde{N}_{even}-1\right)}{2} = \begin{cases} \frac{\left(N^1_{even}+N^2_{even}\right)\left(N^1_{even}+N^2_{even}-2\right)}{8}; & N^1_{even}+N^2_{even} \text{ is even} \\ \frac{\left(N^1_{even}+N^2_{even}\right)^2-1}{8}; & N^1_{even}+N^2_{even} \text{ is odd} \end{cases} \quad (103)$$

and thus, the b constants can be determined by enforcing (101) and/or (101) at a minimum of N_b points.

Substituting for the fields in (99) and (100) as given in the previous section, we obtain the equations

$$V_F^{odd}(\lambda_o, y) = \sum_{p=1}^{N_a} a_p Z_F^{odd}(m(p), n(p), \lambda_o, y) \quad (104)$$

$$V_{\partial xF}^{odd}(\lambda_o, y) = \sum_{p=1}^{N_a} a_p Z_{\partial xF}^{odd}(m(p), n(p), \lambda_o, y) \quad (105)$$

where $a_p = a_{m(p)n(p)}$ with

$$p = \frac{(n+m-1)(m+n)}{2} + m \quad (106)$$

$$m(p) = p - \frac{1}{2} Int\left\{\frac{\sqrt{1+8(p-1)}-1}{2}\right\} \cdot Int\left\{\frac{\sqrt{1+8(p-1)}+1}{2}\right\} \quad (107)$$

$$n(p) = Int\left\{\frac{\sqrt{1+8(p-1)}+1}{2}\right\} - m(p) \quad (108)$$

which are in accordance with the ordering of the a_{mn} constants as the order of the GSTC is increased (see Figure 8). The functions V_F^{odd}, $V_{\partial xF}^{odd}$, Z_F^{odd} and $Z_{\partial xF}^{odd}$ are readily determined from the previous analysis and are not quoted here.

Equations similar to (104) - (105) can be obtained for the b constants in a parallel manner.

8 Validation of the Solution

The validity of the derived angular spectra and diffraction coefficients was already performed to a limited degree in Section 4 of the paper. What remains, therefore, is a validation of the procedure for computing the constants a_{mn} and b_{mn} which amounts to solving a small matrix. The validation was done by comparison with processed data from a numerical model which consisted of a finite length slab having the prescribed discontinuity or junction at its center. First, the transient response of this finite slab was generated from bandlimited frequency domain data. The contribution from the material junction was then obtained by time gating the transient response. Numerically derived data from this procedure were found in good agreement with the presented analytical solution. An example is shown in Figure 9 corresponding to a thick (0.2 freespace wavelengths) material half plane. The numerical and analytical data are clearly in good agreement, and it is again demonstrated that the constants play a major role in the solution.

9 Other Applications of the GIBC/GSTC

It was shown above that the GIBC can effectively model thick planar layers of material. However, corresponding GIBC can also be derived for curved coated surfaces (see Figure 10), and the improved accuracy of these is particularly evident when surface wave effects are dominant. For surfaces having relatively large radii of curvature these can be easily derived from those of the planar surface with x and z replaced by the local tangential variables and y by the normal one. With a second order GIBC derived in this manner, the Mie series and GTD solutions have been found [20], [21] and compared with the exact modal series solution for a coated cylinder. As illustrated in Figure 11, the field given by the Mie series based on the GIBC is in excellent agreement with the exact result even at points close to the surface in the shadow region where a finite order boundary condition is inadequate. In contrast, data based on the standard impedance boundary condition (SIBC) are substantially inaccurate.

Higher order boundary conditions have advantages in numerical treat-

ments as well. When used to simulate a coating, a GIBC eliminates the need to sample inside the dielectric, and this is important when storage is limited. In addition, it may be possible to use a GIBC to transfer a boundary condition to a plane, thereby producing a boundary integral equation of convolution type. In conjunction with an FFT, the equation can be solved iteratively to reduce the storage requirement to $O(n)$ where n is the number of unknowns. As an example, for the three dimensional problem of a cavity in a coated ground plane, a GIBC provides a simple modal as well as a reduction in memory. If the coating is lossy or tapered in thickness, the non-uniqueness due to the terminations is avoided, and the same is true for cavities whose depth tapers to zero. Nevertheless, caution must be exercised when solving the integral equation numerically. The GIBC results in higher order derivatives applied to the Green's function, and even if some can be transferred to the current, the increased singularity of the Green's function makes discretization more difficult. In spite of this, integral equation methods using GIBCs of up to the third oder have been successfully implemented [22].

Appendix: Multiplicative Split Functions

In this appendix we consider the splitting of

$$\mathcal{G}\left(\lambda^2\right) = \mathcal{U}_A\left(\lambda^2\right) + \sqrt{1-\lambda^2}\mathcal{U}_B\left(\lambda^2\right) \tag{109}$$

as a product of two functions, one of which is free of poles, zeros and branch cuts in the upper half of the λ plane and the other having the same properties in the lower half of the λ plane. That is, we seek to write $\mathcal{G}\left(\lambda^2\right)$ in the form

$$\mathcal{G}\left(\lambda^2\right) = \mathcal{G}_+\left(\lambda\right)\mathcal{G}_-\left(\lambda\right) \tag{110}$$

where the superscript + and - indicate an upper or lower function, respectively. Noting that

$$\mathcal{U}_A\left(\lambda^2\right) = \sum_{n=0}^{N_A} A_n\left[1-\lambda^2\right]^n \tag{111}$$

$$\mathcal{U}_B\left(\lambda^2\right) = \sum_{n=0}^{N_B} B_n\left[1-\lambda^2\right]^n \tag{112}$$

with $N_A = N_B$ or $N_A = N_B + 1$, we may rewrite $\mathcal{G}\left(\lambda^2\right)$ as

$$\mathcal{G}\left(\lambda^2\right) = \sum_{n=0}^{N_S} S_n\left[\sqrt{1-\lambda^2}\right]^n \tag{113}$$

where $N_s = Max(2N_A, 2N_B+1)$ and $S_n = A_{n/2}$ if n is even and $S_n = B_{(n-1)/2}$ if n is odd. However, since we seek a multiplicative splitting of (113), a more convenient form to represent $\mathcal{G}\left(\lambda^2\right)$ is

$$\mathcal{G}\left(\lambda^2\right) = S_0\prod_{n=1}^{N_S}\left(1+\frac{\sqrt{1-\lambda^2}}{\gamma_n}\right) \tag{114}$$

in which γ_n denote the zeros of the polynomial $\sum_{l=0}^{N_S} S_l\left(-\lambda\right)^l$. We immediately now identify that each of the product terms in (114) can be factored as

$$1+\frac{\sqrt{1-\lambda^2}}{\gamma} \stackrel{def}{=} M_+\left(\lambda;\gamma\right)M_-\left(\lambda;\gamma\right) \tag{115}$$

where

$$K_+(\lambda;1/\gamma)=\frac{\sqrt{1-\lambda}}{M_+(\lambda;\gamma)} \tag{116}$$

is the split function characteristic to the impedance half plane having a constant surface impedance $1/\gamma$ [17]. With the branch choosen so that $Im(\sqrt{1-\lambda^2})<0$, $M_+(\lambda;\gamma)$ is explicitly given by

$$M_+(\lambda;\gamma)=M_-(-\lambda;\gamma)=\begin{cases}\widetilde{M}_+(\lambda;\gamma) & Im(\gamma)\le 0\\ \frac{j\eta\left(\lambda-\sqrt{1-\gamma^2}\right)}{\widetilde{M}_+(\lambda;-\gamma)} & Im(\gamma)>0,\end{cases} \tag{117}$$

$$\widetilde{M}_+(\cos\alpha;1/\eta)=\frac{\Psi_\pi^4(\pi/2)\left[1+\sqrt{2}\cos\left(\frac{\pi/2-\alpha+\theta}{2}\right)\right]\left[1+\sqrt{2}\cos\left(\frac{3\pi/2-\alpha-\theta}{2}\right)\right]}{\sqrt{\frac{8}{\eta}}\left[\Psi_\pi(3\pi/2-\alpha-\theta)\,\Psi_\pi(\pi/2-\alpha+\theta)\right]^2} \tag{118}$$

In this,

$$\begin{aligned} Im(\eta) &\ge 0\\ \lambda &= \cos\alpha\\ Im\left(\sqrt{1-1/\eta^2}\right) &\le 0\\ \theta &= \sin^{-1}(\eta)\text{ with }0\le Re(\theta),\end{aligned} \tag{119}$$

and $\Psi_\pi(\alpha)$ is the Maliuzhinets function [18] whose evaluation in algebraic form has been given in [19].

The determination of $\mathcal{G}_\pm(\lambda)$ is now rather trivial. By substituting (115) into (114) we easily obtain

$$\mathcal{G}_+(\lambda)=\mathcal{G}_-(-\lambda)=\sqrt{S_0}\prod_{n=1}^{N_S}M_+(\lambda;\gamma_n) \tag{120}$$

References

[1] T. B. A. Senior, "Impedance Boundary Conditions for Imperfectly Conducting Surfaces," *Appl. Sci. Res.*, Vol. 8(B), pp.418-436, 1960.

[2] T. B. A. Senior, "Combined Resistive and Conductive Sheets," *IEEE Trans. on Antennas and Propagat.*, AP-33, No. 5, pp. 577-579, May 1985.

[3] J. Kane and S. N. Karp, "An Accurate Boundary Condition to Replace Transition Condition at Dielectric-Dielectric Interfaces," Institute of Mathematical Sciences Division of E.M. Research, New York University, New York, N. Y., Research Report EM-153, May 1960a.

[4] S. N. Karp and F. C. Karal Jr., "Generalized Impedance Boundary Conditions with Applications to Surface Wave Structures," in Electromagnetic Wave Theory, Part 1, ed. J. Brown, pp. 479-483, Pergamon: New York, 1965.

[5] L. A. Weinstein, The Theory of Diffraction and the Factorization Method, Golem Press: Boulder, CO., 1969.

[6] T. B. A. Senior and J. L. Volakis, "Sheet Simulation of a Thin Dielectric Layer," *Radio Science*, vol. 22, pp. 1261-1271, December 1987.

[7] J. M. L. Bernard, "Diffraction by Metallic Wedge Covered with a Dielectric Material," *Journal of Wave Motion*, Vol. 9, pp. 543-561, 1987.

[8] R. G. Rojas, and Z. Al-hekail, "Generalized Impedance/Resistive Boundary Conditions for Electromagnetic Scattering Problems," *Radio Science*, Vol. 24, No. 1, pp. 1-12, Jan-Feb 1989.

[9] T. B. A. Senior and J. L. Volakis, "Derivation and Application of a Class of Generalized Boundary Conditions," *IEEE Trans. on Antennas and Propagat.*, AP-37, No. 12, December, 1989.

[10] M. A. Ricoy and J. L. Volakis, "Derivation of generalized transition/boundary conditions for planar multiple layer structures," *Radio Science* (in press).

[11] J. L. Volakis, and T. B. A. Senior, "Application of a Class of Generalized Boundary Conditions to Scattering by a Metal-Backed Dielectric Half Plane," *Proceedings of the IEEE*, pp 796-805, May 1989.

[12] T. B. A. Senior, "Diffraction by a Generalized Impedance Half Plane," presented at URSI International Electromagnetic Wave Theory Symposium, Stockholm, Sweden, 14-17 August 1989.

[13] P. C. Clemmow, "A method for the exact solution of a class of two-dimensional diffraction problems," *Proc. Roy. Soc. A*, Vol. 205, pp. 286-308, 1951.

[14] J. L. Volakis, and M. A. Ricoy, "Diffraction by a thick perfectly conducting half-plane," *IEEE Trans. on Antennas and Propagat.*, AP-35, No. 1, pp. 62-72, January, 1987.

[15] M. A. Ricoy and J. L. Volakis, "Diffraction by a Multilayer Slab Recessed in a Ground Plane via Generalized Impedance Boundary Conditions," submitted to *Radio Science.*

[16] V. V. Shevchenko, Continuous Transitions in Open Waveguides, Golem Press: Boulder, CO., 1971.

[17] T. B. A. Senior, "Diffraction by a semi-infinite metallic sheet, *Proc. Roy. Soc.* (London), A213,pp. 436-458, 1952.

[18] G.D. Maliuzhinets, " Excitation, Reflection and Emission Of Surface Waves From a Wedge With Given Face Impedances," *Sov. Phys. Dokl.*, Engl. Transl., 3, 752-755, 1958.

[19] J. L. Volakis and T. B. A. Senior,"Simple expressions for a function occurring in diffraction theory," *IEEE Trans. Antennas Propag.*, vol. AP-33, pp. 678-680, June 1985.

[20] J.L. Volakis and H.H. Syed, "Application of higher order boundary conditions to scattering by multilayer coated cylinders," *J. Electromag. Waves Applics.*, 1991.

[21] H.H. Syed and J.L. Volakis, "Diffraction by coated cylinders using higher order impedance boundary conditions," submitted to *IEEE Trans. Antennas Propagat.*

[22] K. Barkeshli and J.L. Volakis, "TE scattering by a two- dimensional groove in a ground plane using higher order boundary conditions," *IEEE Trans. Antennas Propagat.*, Oct. 1990.

Publications Resulting from this Research

Reports written (to date) related to this task

1. J.L. Volakis, T.B.A. Senior and J.M. Jin, "Derivation and Application of a Class of Generalized Impedance Boundary Conditions - II," University of Michigan Radiation Laboratory Technical Report 025921-1-T, February 1989. 38pp.

2. M.A. Ricoy and J.L. Volakis, "Derivation of Generalized Transition/ Boundary Conditions for the Planar Multiple Layer Structures," University of Michigan Radiation Laboratory, Technical Report 025921-5-T, August 1989. 36pp.

3. H.H. Syed and J.L. Volakis, "An Approximate Skew Incidence Diffraction Coefficient for an Impedance Wedge," University of Michigan Radiation Laboratory Report 025921-4-T.

4. M.A. Ricoy and J.L. Volakis, "Diffraction by a Multilayered Slab Recessed in a Ground Plane via the Generalized Impedance Boundary Conditions," University of Michigan Radiation Laboratory Report 025921-8-T.

5. H.H. Syed and J.L. Volakis, "An Asymptotic Analysis of the Plane Wave Scattering by a Smooth Impedance Cylinder," University of Michigan Radiation Laboratory Report 025921-9-T.

6. M.A. Ricoy and J.L. Volakis, "Electromagnetic Scattering from Two-Dimensional Thick Material Junctions," University of Michigan Radiation Laboratory Report 025921-14-T.

Papers written (to date) related to this task

1. T.B.A Senior and J.L. Volakis, "Derivation and Application of a Class of Generalized Impedance Boundary Conditions," *IEEE Trans. Antennas and Propagat.*, Vol. AP-37, pp. 1566-1572, December 1989.

2. M.A. Ricoy and J.L. Volakis, "Derivation of Generalized Transition/ Boundary Conditions from Planar Multiple Layer Structures," accepted in *Radio Science.*

3. J.L. Volakis and T.B.A. Senior, "Application of a Class of Generalized Boundary Conditions to Scattering by a Metal-Backed Dielectric Half-Plane," *Proceedings of the IEEE*, Vol. 77, No. 5, pp. 796-805, May 1989.

4. H.H. Syed and J.L. Volakis, "An Approximate Skew Incidence Diffraction Coefficient for an Impedance Wedge," submitted to *IEEE Trans. Antennas and Propagat.*

5. M.A. Ricoy and J.L. Volakis, "Diffraction by a Multilayered Slab Recessed in a Ground Plane via the Generalized Impedance Boundary Conditions," submitted to *Radio Science.*

6. M.A. Ricoy and J.L. Volakis, "Diffraction by a Symmetric Material Slab; Part I: General Solution," submitted to *IEEE Trans. Antennas and Propagat.*

7. M.A. Ricoy and J.L. Volakis, "Diffraction by a Symmetric Material Slab; Part II: Resolution of Non-Uniqueness Associated with Higher Order Boundary Conditions," submitted to *IEEE Trans. Antennas and Propagat.*

8. T.B.A. Senior and J.L. Volakis, "Generalized Impedance Boundary Conditions in Scattering," submitted to *Proceedings of the IEEE.*

Conference Papers/Presentations to date related to this task

1. J.L. Volakis and T.B.A. Senior, "Application of a Class of Generalized Boundary Conditions to Scattering by a Metal-Backed Dielectric Half Plane," 1988 Journess International De Nice Sur Les Antennas (JINA), Nice, France; Digest pp. 115-119.

2. J.L. Volakis and T.B.A. Senior, "Generalized Impedance Boundary Conditions for Dielectric Surfaces and Layers," 1989 National Radio Science Meeting, Boulder, CO, Session B-7, January 1989. Digest p. 211.

3. M.A. Ricoy and J.L. Volakis, "Derivation of Generalized Transition/ Boundary Conditions for Planar Multiple Layer Structures," 1990 National Radio Science Meeting, Boulder, CO.

4. H.H. Syed and J.L. Volakis, "An Approximate Diffraction Coefficient for an Impedance Wedge at Skew Incidence," 1989 IEEE AP-S/URSI Symposium, Session 57, San Jose, CA. AP-S Digest pp. 1286-1289.

5. M.A. Ricoy and J.L. Volakis, "Application of Higher Order Boundary Conditions in Scattering by Material Discontinuities," 1989 IEEE AP-S/URSI Symposium, Session 63, San Jose, CA. URSI Digest p. 279.

6. M.A. Ricoy and J.L. Volakis, "Application of Generalized Impedance Boundary Conditions to Diffraction by a Multilayered Metal-Dielectric Junctions," presented at the 1990 IEEE AP-S/URSI Symposium, Dallas, TX, URSI Digest p. 62.

7. H.H. Syed and J.L. Volakis, "Diffraction by a Smooth Coated Cylinder Simulated with Generalized Impedance Boundary Conditions," presented at the 1990 IEEE AP-S/URSI Symposium, Dallas, TX, URSI Digest p. 176.

8. J.L. Volakis and H.H. Syed, "Application of Higher Order Boundary Conditions to Scattering by Multilayered Coated Cylinders," 1990 IEEE AP-S/URSI Symposium, Dallas, TX, AP-S Digest pp. 586-589.

9. M.A. Ricoy and J.L. Volakis, "On the Analytical Implementation of Generalized Impedance Boundary Conditions," to be presented at the 1990 URSI General Assembly, Session B5, Prague, Chechoslovakia.

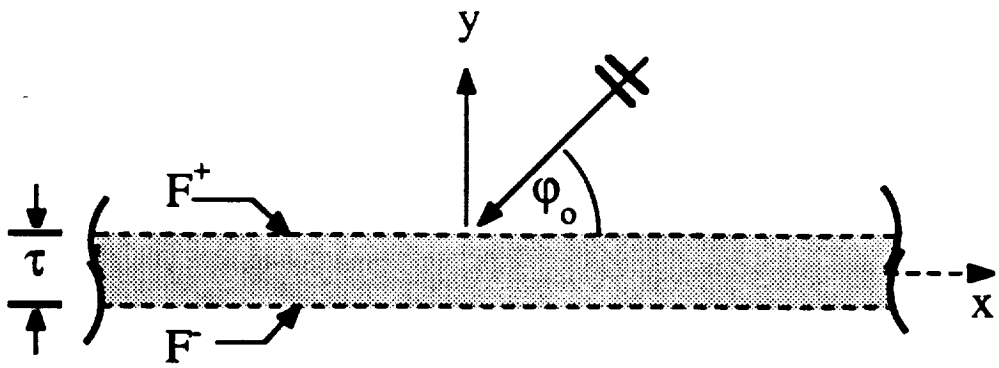

Odd GSTC: $$u_{11}\left(-\frac{\partial x^2}{k^2}\right)\{F^+ - F^-\} + \frac{j}{k}u_{12}\left(-\frac{\partial x^2}{k^2}\right)\partial y[F^+ + F^-] = 0$$

Even GSTC: $$u_{21}\left(-\frac{\partial x^2}{k^2}\right)\{F^+ + F^-\} + \frac{j}{k}u_{22}\left(-\frac{\partial x^2}{k^2}\right)\partial y[F^+ - F^-] = 0$$

(a)

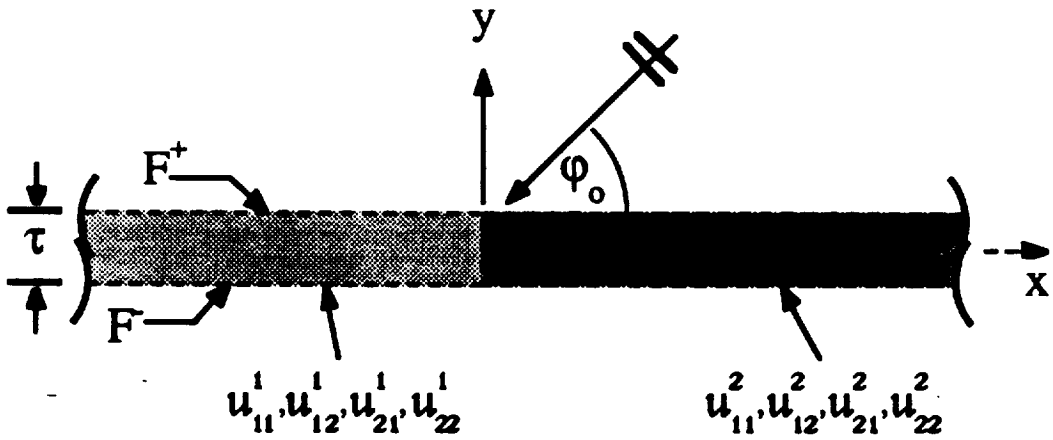

(b)

Figure 1. (a) Distributed sheet. (b) Distributed sheet discontinuity.

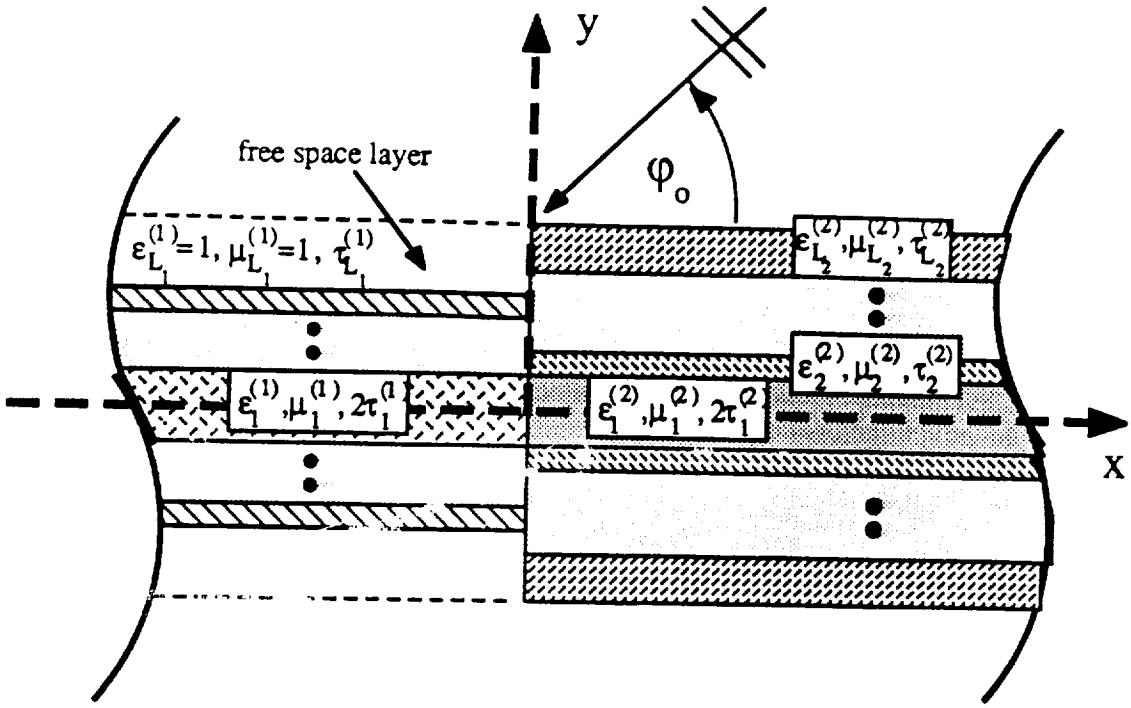

Figure 2. Geometry of the material-material join.

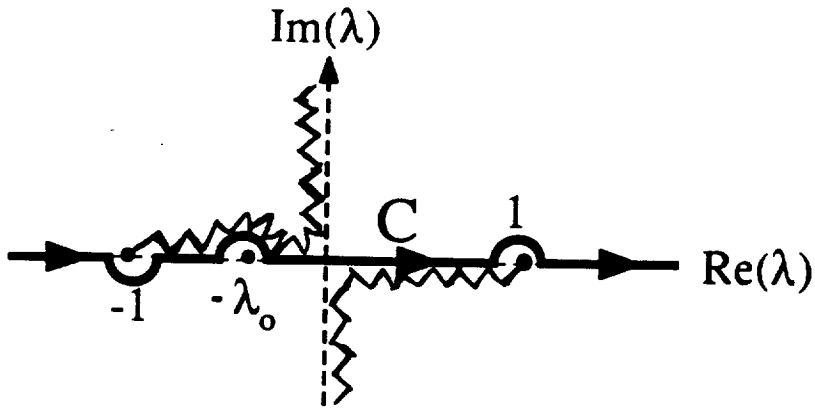

Figure 3. Illustration of the C contour in the complex λ-plane.

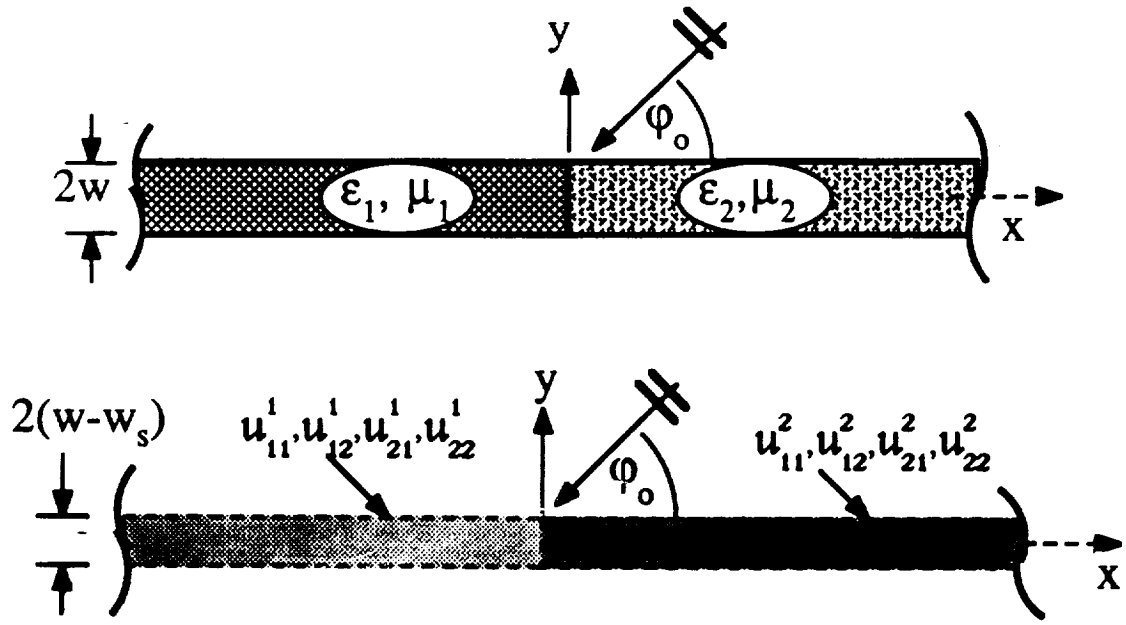

Figure 4. Thin discontinuous slab and its associated sheet representation.

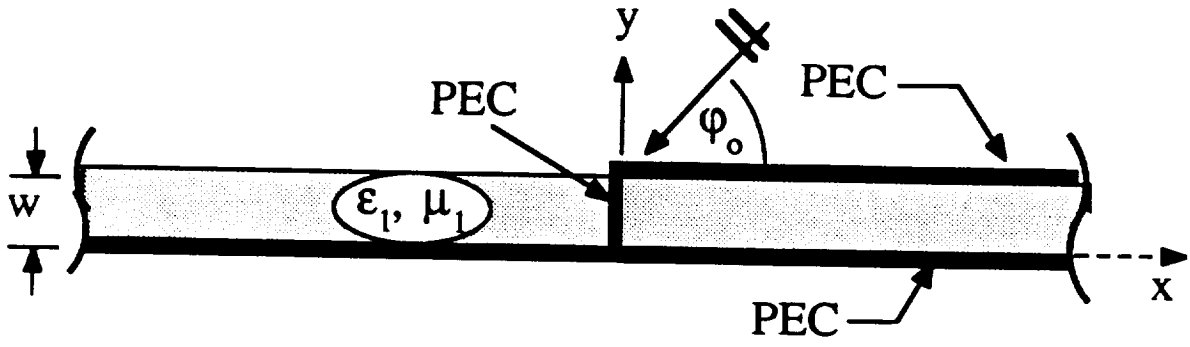

Figure 5. Recessed slab (PEC stub) on a ground plane.

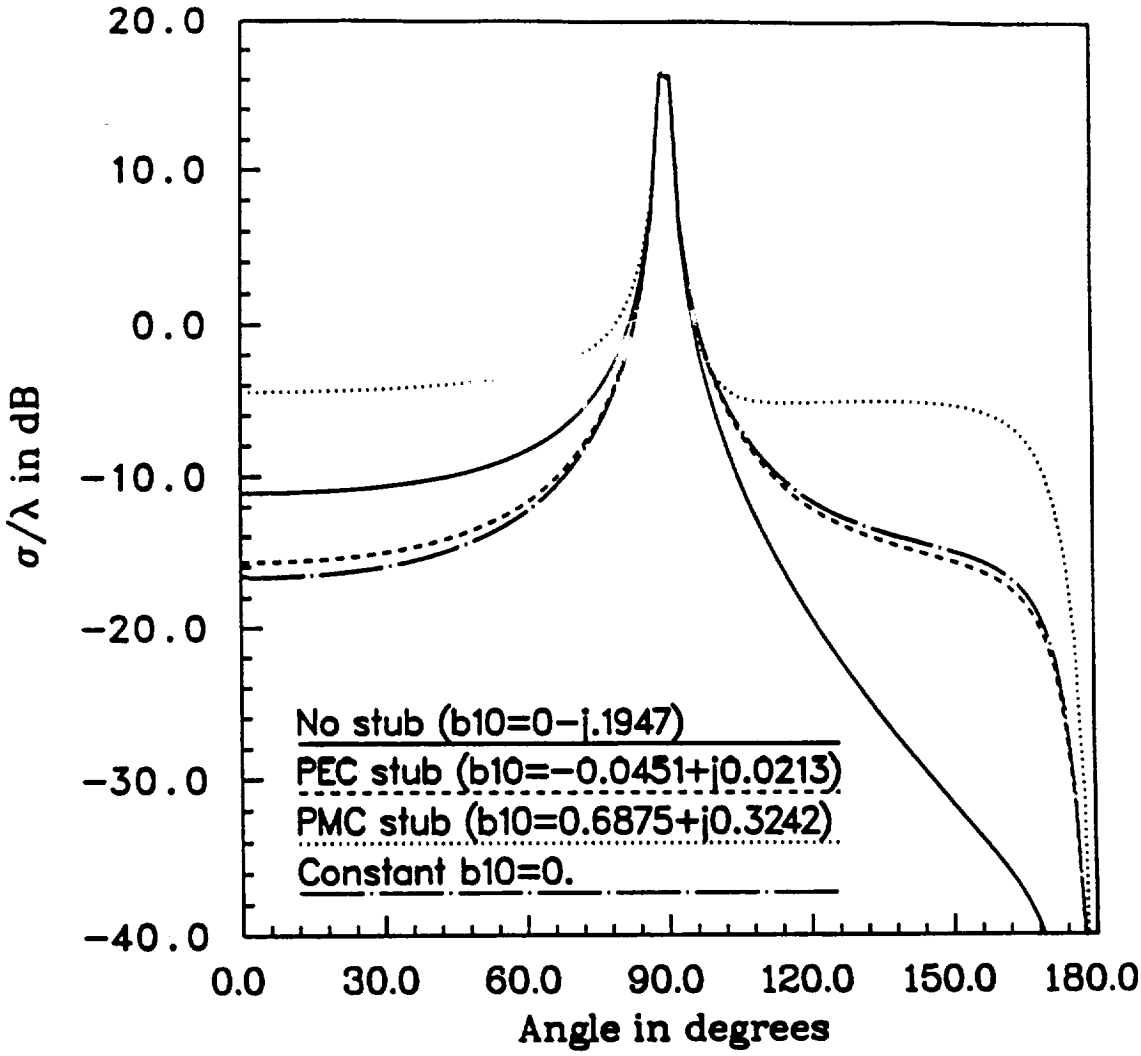

Figure 6. H_z-polarization backscatter echowidth for a material insert having w=0.04λ, ε=2-j.0001, μ=1.2 modeled with O(w) low contrast GIBCs.

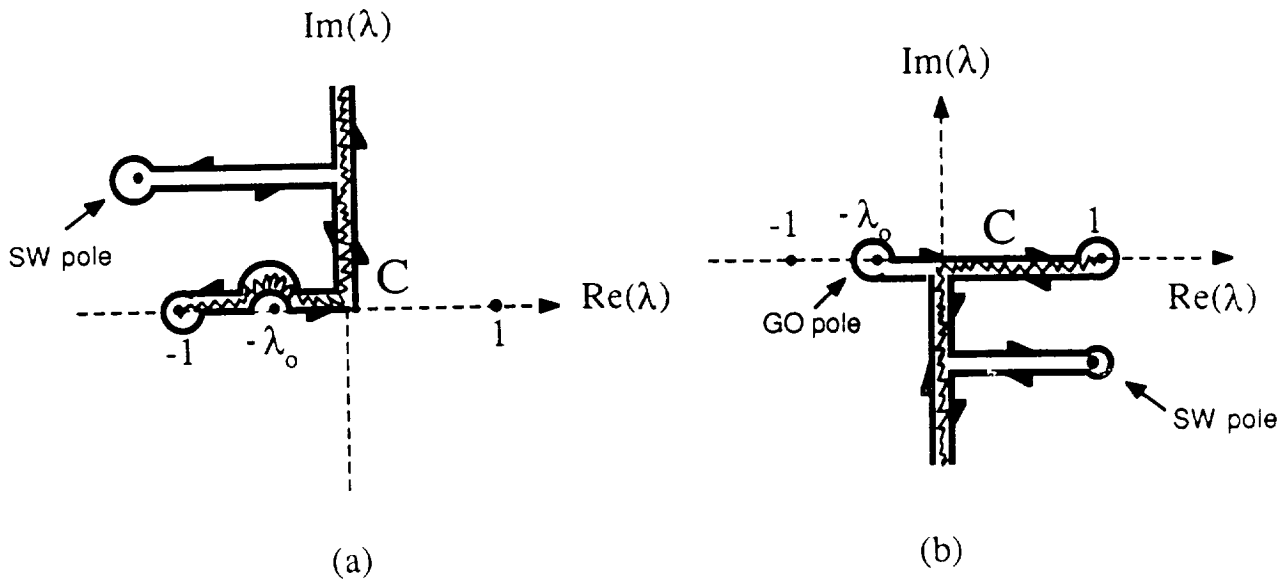

Figure 7. Deformation of the C contour for (a) region 1 integrals and (b) region 2 integrals.

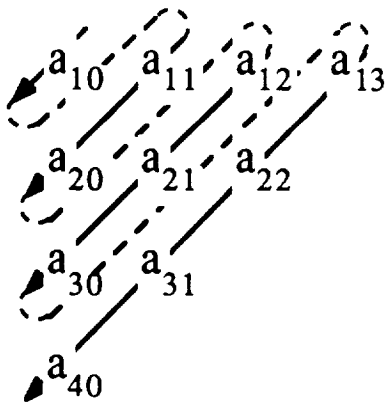

Figure 8. Indexing scheme for the constants.

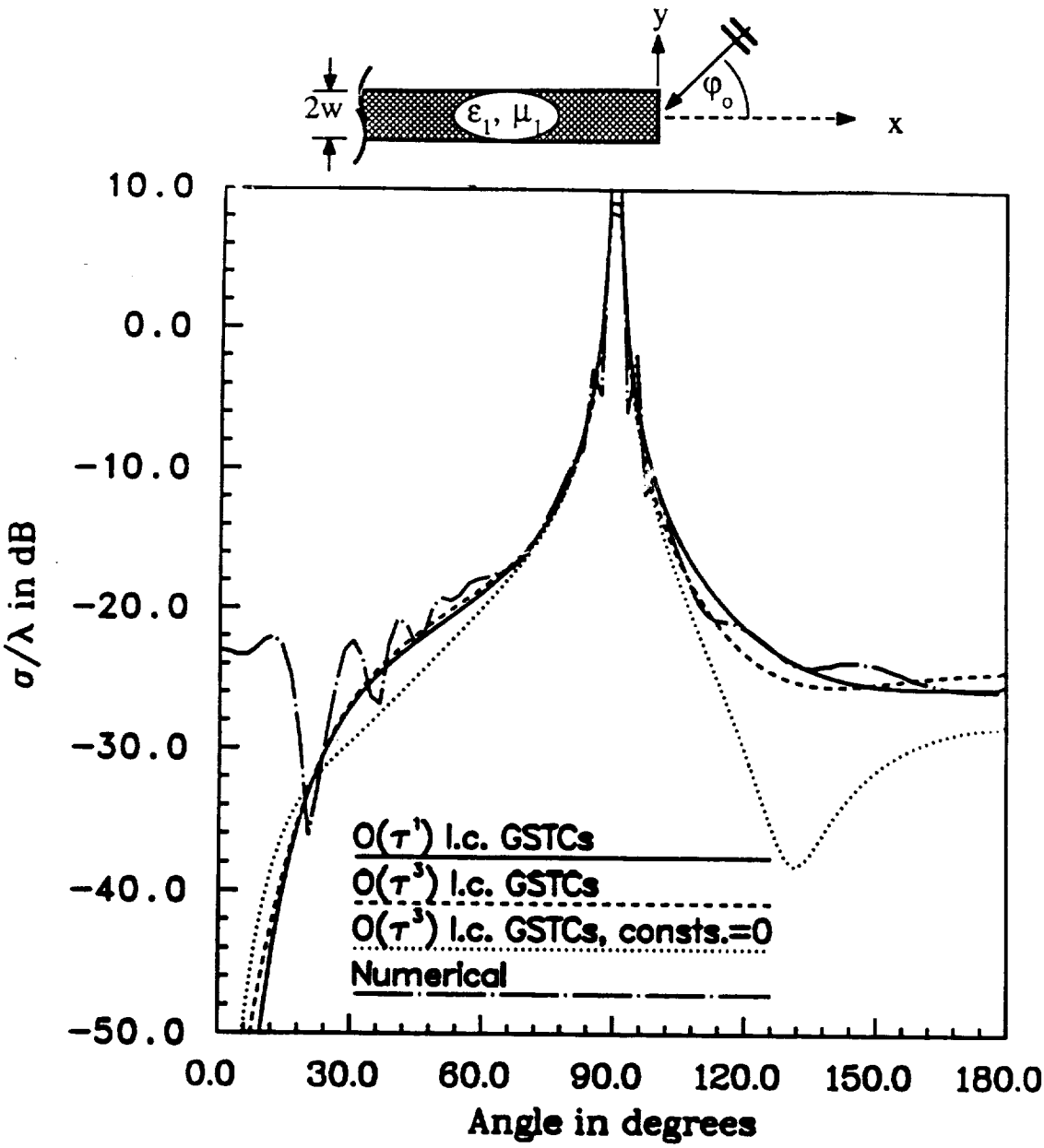

Figure 9. H_z-polarization backscatter echowidth for material half-plane with τ=.20, ε=2-j.0001, μ=1.2.

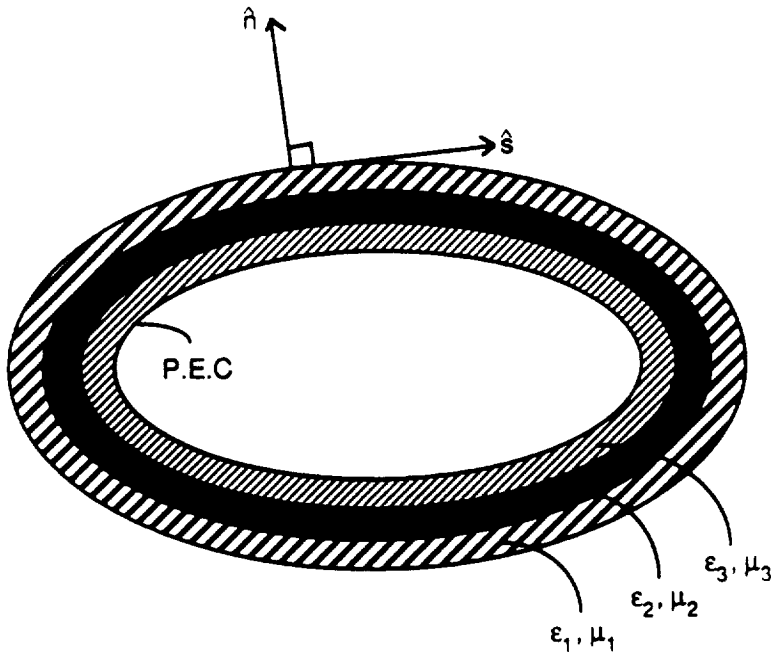

Figure 10. Illustration of a three-layer coated cylinder.

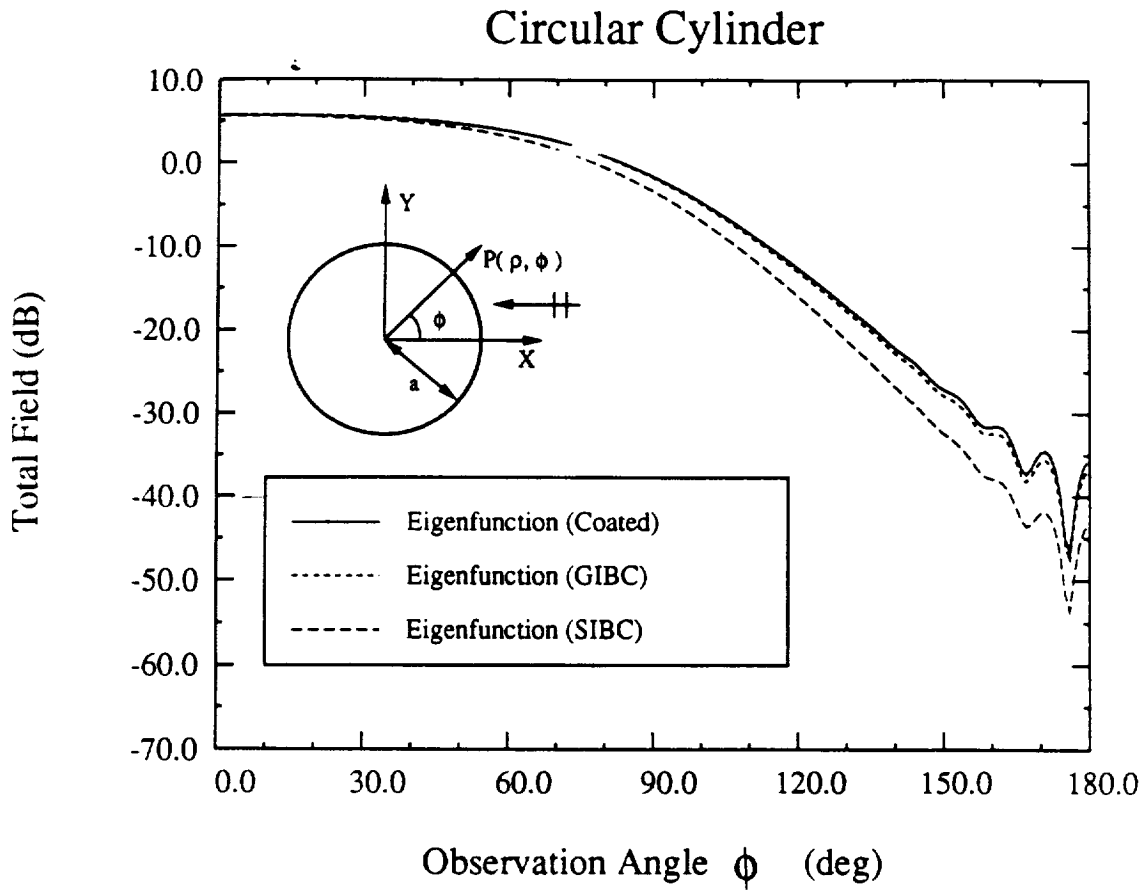

Figure 11. Bistatic H-polarization scattering pattern of a circular cylinder of Radius 2.93λ coated with a layer 0.07λ thick having ε=4 and μ=1; Comparison of fields at a distance 0.05λ away from the coatings surface.

Geometry, $x > 0$	$\mathcal{U}_{11}^2(-\cos\phi\cos\phi_o)$	$\mathcal{U}_{12}^2(-\cos\phi\cos\phi_o)$	$\mathcal{G}_{odd}^{2+}(\cos\phi)\,\mathcal{G}_{odd}^{2+}(\cos\phi_o)$	$\gamma^{odd,2}$
Low Contrast $O(w, w_s)$	1	$jk(u_2 w - w_s)$	$M_+\left(\cos\phi;\gamma_1^{odd,2}\right) M_+\left(\cos\phi_o;\gamma_1^{odd,2}\right)$	$\frac{-j}{k(u_2 w - w_s)}$
Free Space Limit	1	$jk(w - w_s)$	$M_+\left(\cos\phi;\gamma_1^{odd,2}\right) M_+\left(\cos\phi_o;\gamma_1^{odd,2}\right)$	$\frac{-j}{k(w-w_s)}$
PEC(Ez-pol) or PMC(Hz-pol)	1	0	1	———
PMC(Ez-pol) or PEC(Hz-pol)	0	1	$\sqrt{1-\cos\phi}\sqrt{1-\cos\phi_o}$	———

Table 1: Odd symmetry parameters associated with the right hand side material $x > 0$. See Appendix for the definition of the M_+ split functions.

Geometry, $x > 0$	$\mathcal{U}_{21}^2(-\cos\phi\cos\phi_o)$, $\mathcal{U}_{22}^2(-\cos\phi\cos\phi_o)$	$\mathcal{G}_{even}^{2+}(\cos\phi)\,\mathcal{G}_{even}^{2+}(\cos\phi_o)$
Low Contrast, $O(w, w_s)$	$\mathcal{U}_{21}^2 = jk\left(\frac{w\epsilon_2\mu_2}{u_2} - w_s\right)$ $+jk\cos\phi\cos\phi_o\left(\frac{w}{u_2} - w_s\right)$ $\mathcal{U}_{22}^2 = 1$	$\frac{jkw}{u_2}(\epsilon_2\mu_2 - 1)\prod_{m=1}^{2} M_+(\cos\phi;\gamma_m^{even,2}) M_+(\cos\phi_o;\gamma_m^{even,2})$ with $\gamma_{1,2}^{even,2} = \frac{u_2 \pm \sqrt{u_2^2 + 4k^2 w(\epsilon_2\mu_2 - 1)(w - u_2 w_s)}}{2jk(w - w_s u_2)}$
Free Space Limit	$\mathcal{U}_{21}^2 = jk(w - w_s)(1 + \cos\phi\cos\phi_o)$ $\mathcal{U}_{22}^2 = 1$	$\sqrt{1-\cos\phi}\sqrt{1-\cos\phi_o} M_+\left(\cos\phi;\gamma_1^{even,2}\right) M_+\left(\cos\phi_o;\gamma_1^{even,2}\right)$ with $\gamma_1^{even,2} = \frac{-j}{k(w-w_s)}$
PEC(Ez-pol) ($b_{10} = 0$) or PMC(Hz-pol) ($b_{10} = 0$)	$\mathcal{U}_{21}^2 = 1$ $\mathcal{U}_{22}^2 = 0$	1
PMC(Ez-pol) or PEC(Hz-pol)	$\mathcal{U}_{21}^2 = 0$ $\mathcal{U}_{22}^2 = 1$	$\sqrt{1-\cos\phi}\sqrt{1-\cos\phi_o}$

Table 2: Even symmetry parameters associated with the right hand side material $x > 0$. See Appendix for the definition of the M_+ split functions.